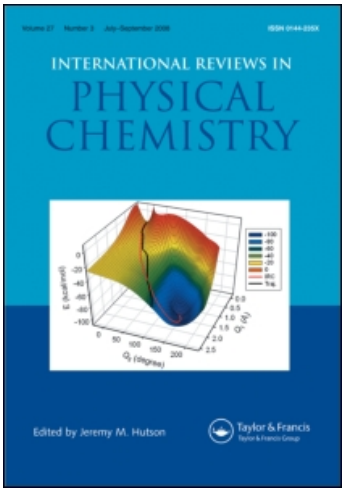

International Reviews in Physical Chemistry
Publication details, including instructions for authors and subscription information:
http://www.informaworld.com/smpp/title~content=t713724383

Microscopic molecular optics theory of surface second harmonic generation and sum-frequency generation spectroscopy based on the discrete dipole lattice model

De-Sheng Zheng[a]; Yuan Wang[a]; An-An Liu[a]; Hong-Fei Wang[a]
[a] Beijing National Laboratory for Molecular Sciences, State Key Laboratory of Molecular Reaction Dynamics, Institute of Chemistry, Chinese Academy of Sciences, Beijing, China

To cite this Article Zheng, De-Sheng , Wang, Yuan , Liu, An-An and Wang, Hong-Fei(2008) 'Microscopic molecular optics theory of surface second harmonic generation and sum-frequency generation spectroscopy based on the discrete dipole lattice model', International Reviews in Physical Chemistry, 27: 4, 629 — 664
To link to this Article: DOI: 10.1080/01442350802343981
URL: http://dx.doi.org/10.1080/01442350802343981

International Reviews in Physical Chemistry
Vol. 27, No. 4, October–December 2008, 629–664

Taylor & Francis
Taylor & Francis Group

Microscopic molecular optics theory of surface second harmonic generation and sum-frequency generation spectroscopy based on the discrete dipole lattice model

De-Sheng Zheng[1], Yuan Wang[2], An-An Liu[1] and Hong-Fei Wang*

Beijing National Laboratory for Molecular Sciences, State Key Laboratory of Molecular Reaction Dynamics, Institute of Chemistry, Chinese Academy of Sciences, Beijing, China

(*Received 14 June 2008; final version received 11 July 2008*)

The aim of this work is to present a coherent description of the microscopic theory of surface nonlinear optical spectroscopy for solving practical problems in understanding the details of the molecular interface. We review the related issues and show that by following microscopic molecular optics theory, second harmonic generation (SHG), as well as sum-frequency generation vibrational spectroscopy (SFG-VS), radiation from a monolayer or submonolayer can be rigorously treated as the radiation from an induced dipole lattice at the interface. In this approach, the introduction of an infinitesimally thin polarization sheet as in macroscopic theory with the Maxwell equations and the boundary conditions is no longer necessary. As a direct consequence, the ambiguity of the unaccounted dielectric constant of the interfacial layer is no longer an issue. Moreover, the anisotropic two-dimensional microscopic local field factors can be explicitly defined with the linear polarizability tensors of the interfacial molecules. Based on the planewise dipole sum rule in the molecular monolayer, experimental tests of this microscopic treatment with SHG and SFG-VS are discussed.

Keywords: interface; submonolayer; molecular orientation; second harmonic generation (SHG); sum frequency generation vibrational spectroiscopy (SFG-VS); Maxwell equations

Contents

*Corresponding author. Email: hongfei@iccas.ac.cn
[1]Graduate students of Graduate School of the Chinese Academy of Sciences.
[2]Exchange graduate student from the Department of Physics, Anhui Normal University, Wuhu, China 241000.

ISSN 0144–235X print/ISSN 1366–591X online

DOI: 10.1080/01442350802343981
http://www.informaworld.com

1. Scope

The aim of this work is to present a coherent description of the microscopic theory of surface nonlinear optical spectroscopy for solving practical problems in understanding the details of the molecular interface. In two recent review articles [1,2], one of which was published in this review journal, we reviewed some of the theoretical and experimental issues in the quantitative analysis and interpretation of surface second harmonic generation (SHG) and sum-frequency generation vibrational spectroscopy (SFG-VS) based on the macroscopic theory of the surface SHG and SFG-VS. This work intends to add some new flavour to these previous works by presenting a microscopic molecular optics theory of the surface SHG and SFG-VS. With this microscopic description, some of the incompatible issues in the macroscopic theory are dealt with and more detailed molecular level understanding of the molecular interface with nonlinear spectroscopy can also be developed.

The past two and half decades have witnessed tremendous advancement and applications of the interface specific second order nonlinear optical techniques, mainly surface SHG and SFG-VS, in molecular interface studies [1–25]. To put it simply, SHG is a second order nonlinear process where two photons with the same fundamental frequency (ω) interact with a nonlinear medium simultaneously to generate a photon with the second harmonic frequency (2ω). If the two fundamental frequencies are not the same, a photon at the sum of these two frequencies can be generated from the so-called SFG process.

Because of the symmetry requirement for the second order nonlinear processes, the leading dipolar term of the SHG or the SFG processes is generally forbidden for a centrosymmetric bulk medium. Thus, SHG and SFG become effective probes for the interface between the two centrosymmetric bulk phases [26]. The theoretical foundation and the experimental demonstration of the interfacial selectivity of SHG as well as SFG have been pioneered by Shen and his colleagues since the early 1980s [27–34], extending from the original formulation of light waves at the boundary of nonlinear media by Bloembergen *et al*. in the early 1960s [35].

With SHG and SFG-VS, the equilibrium and dynamic behaviour of the molecular interface or film can be directly measured from the nonlinear electronic or vibrational spectroscopic response of the interfacial molecular moieties [4,10–13,25]. One particular aspect of the studies in the past few years has been focused on the quantitative measurement and interpretation of the molecular orientation and vibrational spectra from the SHG and SFG-VS measurements on various molecular interfaces [1,2,36–38]. Recent work also demonstrated that the coherent nature of the surface SHG and SFG-VS processes makes them more advantageous over the other incoherent spectroscopic techniques used in surface studies. The interference of the molecular electric field and the strong polarization dependence in the SHG and SFG-VS response can be employed to investigate the detailed interactions and to determine the molecular conformations at the molecular interfaces [39–41].

However, researchers have long realized that the two crucial issues in quantitative interface studies with SHG and SFG are on how to describe the macroscopic dielectric constant of the molecularly thin layer and on how to quantitatively evaluate the anisotropic two-dimensional microscopic local field effect [1,2,42–54]. It has been well demonstrated that in the majority of cases the calculation of the molecular orientation is quite sensitive to the values used for these two factors [1,2,51–53].

Moreover, closer examination shows that these two issues are conceptually incompatible with each other because the currently accepted theory of surface nonlinear optics is essentially a macroscopic theory, in which the nonlinear radiation was treated as the result of an infinitesimally thin polarization layer or sheet. In this macroscopic theory the Maxwell equations with the boundary conditions of a three-layer model were generally employed. The direct consequence of this approach is that an a priori dielectric constant, which still does not have a clear microscopic definition, has to be assigned to this interfacial polarization layer. This incompatibility has actually limited the understanding and interpretation of the quantitative SHG and SFG-VS data for obtaining more detailed information on the interfacial molecules. To resolve this incompatibility, a microscopic theory of the SHG and SFG-VS is in demand.

Here is how this report is to be arranged. After reviewing the background issues and the related problems, we shall show that a microscopic theory of the SHG/SFG radiation can be rigorously presented along with a discrete dipole lattice model. In the field far from the discrete dipole lattice the SHG/SFG radiation is in the same form as in the infinitesimally thin polarization sheet layer model, validating previously developed macroscopic SHG/SFG theory. Moreover, in this microscopic theory, the introduction of the polarization sheet is no longer necessary. Therefore, the ambiguity of the unaccounted dielectric constant of the polarization layer is no longer an issue. Incidentally, the anisotropic two-dimensional microscopic local field factors can be explicitly expressed with the linear polarizability

tensors of the interfacial molecules. Based on the planewise dipole sum rule in the molecular monolayer, crucial experimental tests of this treatment with the SHG and SFG-VS experiments are discussed. We shall also discuss the puzzles in the literature of the surface SHG and SFG spectroscopy studies as discussed above. This microscopic treatment can provide a consistent theoretical basis for future applications of the quantitative analysis of the surface SHG and SFG for more detailed molecular level interface studies.

2. Background

There have been incompatibilities in the current macroscopic theory on the SHG/SFG in dealing with the microscopic properties of the monolayer and submonolayer molecular interface. In particular, the treatment of the interface dielectric constant and the local field factors has been an unsettled issue [1,2,42,54]. We intend to introduce the microscopic molecular optics theory by Wolf *et al.* into SHG/SFG theory to address these issues [55,56].

2.1. *Problems with the interfacial layer models and the local field factors in the quantitative analysis of SHG/SFG*

In the currently accepted models of the nonlinear optics of interfaces [6,34,42,54,57,58], the nonlinear radiation was treated as the result of an infinitesimally thin polarization sheet layer, and as the starting point a macroscopic dielectric constant was assigned to this thin layer [6,34,57,58]. This model was a natural extension of the original formulation by Bloembergen and Pershan, where a nonlinear plane parallel slab with a finite thickness embedded between two linear dielectrics was the source of the SHG radiation. Then Maxwell's equations which satisfy the boundary conditions at the two plane interfaces were solved [35]. However, Bloembergen and Pershan concluded that the surface dipolar contribution to the SHG signal should be overwhelmed by the quadrupolar radiation in the much thicker boundary layer, i.e. the bulk region in the vicinity of the interface. Contrary to this conclusion, later experimental observations demonstrated that the surface dipolar contribution could be dominant in many cases. By solving Maxwell's equations which satisfy the boundary conditions at the infinitesimally thin polarization sheet layer, Heinz and Shen laid the theoretical foundation for the interface specific SHG, as well as the SFG-VS, for their applications in interface studies [6,34,57,58].

Parallel to this macroscopic treatment, Ye and Shen employed a classical induced point-dipole model to include the microscopic local field effect on the nonlinear optical properties of the adsorbed molecules on a substrate [59]. Shen *et al.* later realized that from the theoretical point of view, the dielectric constant in the macroscopic model is not well defined for a monolayer because it is only a macroscopic or mesoscopic property. Thus, Shen *et al.* tried to phenomenologically interpret this macroscopic dielectric constant as a result of the microscopic local field correction in a monolayer, and they also gave explicit expressions for the macroscopic Fresnel factors and the microscopic local-field factors [42,54]. In one case, Zhuang *et al.* also demonstrated that in a Langmuir monolayer it is satisfactory to treat the whole molecule with one unique microscopic local field factor derived using a modified Lorentz three-layer model of the interface [54]. This approach has been widely followed for quantitative interpretation of the SHG and the SFG-VS data since [1,2].

However, puzzles and confusions have remained in the SHG and SFG-VS practices on how the linear macroscopic dielectric constant and the microscopic local field factors, as described by Ye and Shen, should be used in the quantitative treatment of the experimental data. In their SHG study of the self-assembled monolayer (SAM) on a gold substrate, Eisert *et al*. carefully compared the results with the macroscopic three-layer model and the two-layer model, as well as the local field corrections. They concluded that using the two-layer model without local-field correction gave most satisfactory agreement on the molecular orientation with the results from the NEXAFS and IR spectroscopy measurements [52]. This work is obviously not consistent with the above treatment by Shen *et al*. It was further criticized by Roy on the inconsistency that the SAM film was considered anisotropic for SHG but assumed to be isotropic in terms of its linear optical properties [60].

Roy then outlined a macroscopic phenomenological model that treated the linear and nonlinear optics of the anisotropic interface layer in a single framework, which nevertheless requires a minimum of six unknown parameters of the interfacial optical constants even for a uniaxial monolayer in the SHG or the SFG-VS formulation [60,61]. Thus, Roy concluded that the conventional SHG measurement of phase and intensity may not be enough to determine the orientation of SAM. However, even though the anisotropy is undoubtedly significant on the nonlinear responses, Roy's criticism might have exaggerated the influence of the anisotropy on the linear optical properties within the monolayer, which in fact only slightly modifies the reflectivity of the surface as judged from ellipsometry measurements. [26,62–64].

There have been a few experimental and empirical theory studies on the SHG data of the interfacial monolayer, using different parameters of the macroscopic three-layer model plus the microscopic local field factors [43–50,52,65–67]. In some cases, generally one of the two bulk phase values were used as the interfacial macroscopic dielectric constant, reducing the macroscopic problem to the same as the so-called two-phase model [68,69]. However, because the two-phase model does not consider the different microscopic properties of the surface molecular layer, it can only phenomenologically describe the surface SHG process, and it generally fails to quantitatively explain the observed differences in the SHG measurement. On the other hand, in dealing with the microscopic local field factors, some works followed the classical dipole model as presented by Ye and Shen, and the rest followed the simple Lorentz–Lorenz local field expression using the bulk polarizabilities [66,67].

Another approach completely neglected the treatment of the microscopic local field effect, and treated the molecular film with a macroscopic three-layer model [51,53,61,70–74]. In SFG-VS, some considered the film anisotropic, and its optical constant was determined using the Clausius–Mossotti relationship with the ellipsometry data of the film [74]. This apparently resulted from the practice of ellipsometry studies, where it has been generally believed that the macroscopic optical model can be valid down to the monolayer level [62,63]. In SHG, some considered the film isotropic and the optical constant can be obtained from the Kramers–Kronig dispersion relationship measured from the bulk or thin film UV-Visible absorption spectra [51,72,73]. When the molecule is considered with uniaxial symmetry, the ratio between the dielectric constants of the fundamental and the SH frequency can be directly determined from the intensity ratio in the polarization measurements [37,51]. There are also efforts trying to show that

the dielectric constant of the extremely thin monolayer is just the simple arithmetic average of the two bulk dielectric constants [53,61,70,71]. Even though the results from these approaches seemed qualitatively reasonable, neglecting the anisotropic microscopic local field effects in the molecular monolayer is not likely to be physically sound and quantitatively reliable.

The molecular orientation obtained from the above approaches from the SHG and SFG-VS experimental data showed a similar trend. However, the values of the orientational angle depended quite significantly on the different parameters and surface models used. Besides all the different approaches in the SHG and SFG-VS data analysis, experimental studies have shown that the original treatment given by Heinz and Shen with the infinitesimally thin polarization sheet layer is generally correct. On the other hand, researchers in the field also agree that the definition of the dielectric constant of the monolayer or even submonolayer film is unclear and meaningless in macroscopic optics, because when the film is as thin as one molecular layer the macroscopic reflection and transmission coefficients simply converge to the bare interface limit [61–63]. Therefore, even though the treatment provided by Shen and coworkers is generally valid, many issues still need to be clarified. The key problem in the existing model is that the macroscopic and microscopic linear optical properties of the nonlinear molecular layer are not compatible. In practice a more detailed microscopic theory is needed to help understand the detailed SHG or SFG-VS responses from different molecules or different molecular groups in the molecular interface or film.

A similar problem has also existed in the polarized attenuated total internal reflection-Fourier transform infrared (ATR-FTIR) spectroscopy measurement of the orientation of molecular groups in molecular and biological films [75–76]. It was shown that in ATR-FTIR studies the simplest two-layer model may give more consistent orientation angles than those from the more widely used three-layer model [75,78]. Such puzzles in both linear and nonlinear spectroscopic surface studies certainly call for a microscopic theory in order to better quantitatively understand and to test the existing surface dielectric models.

Aside from the above, a microscopic theory of molecular crystal surface SHG was proposed by Munn in the early 1990s [79]. In this formulation, since the surface SHG response is treated microscopically as a sum of responses from the successive surface layers, the introduction of a dielectric constant of the surface layer was not required, and this incidentally yielded a microscopic expression of the dielectric constant of the surface layer. Subsequent studies by Munn and coworkers used the planewise sum rules in molecular crystal dielectric theory [80–85] to simulate the linear and nonlinear optical responses of the model Langmuir–Blodgett films [49,86–89]. In this treatment, Munn *et al.* concluded that improper treatment of the local fields can result in significant errors in the determination of the molecular angle from the SHG data [86,87]. They also showed that in order not to overestimate the microscopic local field factors for the closely packed monolayer films, the monolayer itself had to be segmented into several layers [49,89]. In the microscopic theory, the microscopic local field factors depend on the orientation and distribution of the interfacial dipoles, and the microscopic local field factors are needed to determine the dipole orientation from the SHG data. Therefore, Pannhuis and Munn suggested that a self-consistent approach needs to be employed to solve the problem [87]. This microscopic theory and simulations certainly provided new insights into the treatment of the SHG from the molecular monolayer as well as multilayers.

These insights may contain answers to the questions raised above. However, the implications of these works are yet to be picked up by practitioners in related fields.

2.2. *Microscopic molecular optics theory and the discrete dipole lattice model approaches to the surface SHG/SFG*

SHG and SFG-VS have been proven to be sensitive enough to probe interfacial adsorbates with submonolayer coverage [4,6,11,12]. A question naturally arises about whether the interface with adsorbates in the submonolayer coverage can be treated as a continuously thin layer or sheet with the macroscopic theory. One step further: as the interface coverage increases up to a full monolayer, the question is how the linear and nonlinear optical properties of the interface layer should be described. To answer these questions, the treatment based on the discrete induced dipole model seems to be more realistic. The theoretical tool to be employed is the so-called microscopic molecular optics theory.

According to Born and Wolf, molecular optics theory can directly connect the macroscopic optical phenomena to the molecular properties, and can provide deeper physical insight into electromagnetic interaction problems than does the rather formal approach based on Maxwell's phenomenological equations [55,56]. Therefore, in contrast to the infinitesimally thin polarization sheet layer model treated on the basis of the Maxwell theory, a molecular optics treatment can be developed to describe the coherent SHG or SFG-VS radiation from a discrete lattice in between the two isotropic phases. In this work we shall show that even though there are no general methods to solve the integro-differential equations of molecular optics, the summation, or integration, of the radiation in the far field from a discrete induced dipole lattice can be rigorously solved with the application of the principle of the stationary phase for SHG/SFG theory [56].

The discrete induced dipole lattice model is a more realistic description of the molecular interface than the infinitesimally thin polarization sheet layer model [90]. According to the Ewald–Oseen extinction theorem in molecular optics, there exists only the incident field in vacuum and the dipolar microscopic radiation field in vacuum emitted from each induced dipole [35,55,56]. The calculation of the SHG or SFG-VS radiation from the interface using the integro-differential equations can thus be greatly simplified from the linear optical processes. This is because the SHG and the SFG-VS processes are known with interface selectivity, and the summation or integration of the second harmonic or sum-frequency radiation fields is only over the two-dimensional discrete interfacial induced dipoles, instead of over the whole physical space.

Now, the whole SHG and SFG problem is treated microscopically as radiation from the discrete induced dipoles. The total nonlinear radiation is calculated through summation, or integration, over the whole dipole lattice. Thus, there is no need to use the Maxwell equations together with the boundary conditions as in the infinitesimally thin polarization sheet layer model. This should work because it is known that the Ewald–Oseen extinction theorem just replaces the role of the boundary condition [55]. Therefore, there is no need to use the boundary conditions, where a macroscopic dielectric constant has to be given a priori in order to apply the boundary conditions for a finite volume cell across the boundary area which contains the molecular monolayer. Consequently, the macroscopic dielectric constant for the molecular monolayer, which cannot be defined and is a nuisance parameter in the macroscopic theory, simply disappears in the microscopic theory.

In their classic paper on nonlinear optics, Bloembergen and Pershan [35] showed that the approach using the integral equation based on the Ewald–Oseen extinction theorem reached exactly the same results for the nonlinear response from the nonlinear plate parallel slab [35,91]. Since in that work the slab was treated as the continuous medium, the molecular optics approach was more complex and was simply redundant to the macroscopic theory, i.e. no additional physical insight was reached beyond the macroscopic approach. In contrast, when the microscopic molecular optics approach is combined with the discrete dipole lattice model, it can directly connect the microscopic molecular properties and the macroscopic optical phenomenon. The benefit is not only the consistency in the theoretical treatment as discussed above, but also the possibility of having a microscopic molecular theory for the surface nonlinear optics for future applications in understanding the molecular level details at the molecular interface.

In the next two sections, the detailed step-by-step derivations using the discrete point-dipole model and the molecular optics approach to calculating the SHG and SFG radiation from the two-dimensional dipole lattice are presented. Since the final macroscopic expressions are expected to be the same as obtained from the macroscopic theory using the Maxwell equations and macroscopic boundary conditions, only through these detailed derivations, the physical insights and the connections between the molecular and macroscopic optical properties of the molecular optics theory can be unambiguously revealed. The derivations are presented in a deductive way in order to make it easier for the readers to follow.

3. Linear and nonlinear induced dipole and the local field factors of the monolayer with the discrete point-dipole lattice model

Here we derive the expressions of the linear and nonlinear induced dipole and the local field factors of the monolayer with the discrete point-dipole lattice model. Some aspects of the discussions below can be found in the earlier paper by Ye and Shen [59].

3.1. *Linear and nonlinear induced dipole of the monolayer*

In classical molecular optics, the response of the medium to the incident field is described by means of the electric-dipole moments that are induced in the molecules of the medium under the action of the incident field [55,56]. When an optical field at a frequency ω is incident on a medium, it creates an induced dipole at the incident frequency and its higher harmonics in that medium through the total field that each dipole or molecule experiences. This total field is called the local field $\vec{E}_{\mathrm{loc}}$. The higher harmonic induced dipole can be viewed as the results of multiple interactions with the local optical field. Therefore, they are only strong enough for detection when the optical field is intense enough. The induced dipole at the incident frequency is the source of the radiation in the linear processes, while the others are the source responsible for the radiation in the nonlinear processes. To put it simply, one has

$$\vec{\mu}_{\mathrm{induced}} = \vec{\mu}^{\mathrm{linear}}_{\mathrm{induced}} + \vec{\mu}^{\mathrm{nonlinear}}_{\mathrm{induced}}. \tag{1}$$

Nonlinear optics has been extensively studied since the invention of the first laser in the early 1960s [26,92]. Here we only discuss the linear and the second harmonic process in an optical medium. Considering the fact that both fields in the linear frequency and the resulted second harmonic can contribute to the induced dipole at the second harmonic frequency, one has

$$\begin{aligned}\mu_i &= \mu_i^{\omega} + \mu_i^{2\omega} \\ &= \begin{pmatrix} \alpha_{ix}^{\omega} & \alpha_{iy}^{\omega} & \alpha_{iz}^{\omega} \end{pmatrix} \begin{pmatrix} E_{\mathrm{loc},x}^{\omega} \\ E_{\mathrm{loc},y}^{\omega} \\ E_{\mathrm{loc},z}^{\omega} \end{pmatrix} + \begin{pmatrix} E_{\mathrm{loc},x}^{\omega} & E_{\mathrm{loc},y}^{\omega} & E_{\mathrm{loc},z}^{\omega} \end{pmatrix} \begin{pmatrix} \beta_{ixx} & \beta_{ixy} & \beta_{ixz} \\ \beta_{iyx} & \beta_{iyy} & \beta_{iyz} \\ \beta_{izx} & \beta_{izy} & \beta_{izz} \end{pmatrix} \begin{pmatrix} E_{\mathrm{loc},x}^{\omega} \\ E_{\mathrm{loc},y}^{\omega} \\ E_{\mathrm{loc},z}^{\omega} \end{pmatrix} \\ &\quad + \begin{pmatrix} \alpha_{ix}^{2\omega} & \alpha_{iy}^{2\omega} & \alpha_{iz}^{2\omega} \end{pmatrix} \begin{pmatrix} E_{\mathrm{loc},x}^{2\omega} \\ E_{\mathrm{loc},y}^{2\omega} \\ E_{\mathrm{loc},z}^{2\omega} \end{pmatrix}. \end{aligned} \tag{2}$$

Here α_{ij} is the linear polarizability tensor and β_{ijk} is the second order nonlinear polarizability tensor of the each molecule in the laboratory coordinates $\lambda(x, y, z)$ with the index *ijk* as either one of the three laboratory Cartesian coordinates. The first term in Equation (2) is the linear induced dipole, the second term is the induced dipole at the second harmonic frequency (2ω) induced by the field with the fundamental frequency ω through the second harmonic process, and the third term is the induced dipole at 2ω induced by the field with 2ω through a linear process. The field with 2ω in the third term is the result of the second term. The molecular polarizability tensors in the laboratory coordinate system $\lambda(x, y, z)$ can be projected from the molecular polarizability tensors in the molecular coordinate system $\lambda'(a, b, c)$.

The above is general for any dielectric medium. In the problem we describe below, only the induced dipoles at the interface with the fundamental and second harmonic frequency are considered. The case for the sum-frequency works similarly following the same approach. For the isotropic molecular monolayer, there are two independent linear optical polarizability tensors in the laboratory coordinate system, $\lambda(x, y, z)$, $\alpha_{xx} = \alpha_{yy}$, and α_{zz}; and there are three non-vanishing independent β elements, $\beta_{xxz} = \beta_{yyz} = \beta_{xzx} = \beta_{yzy}$, $\beta_{zxx} = \beta_{zyy}$ and β_{zzz} [2,54]. Now the induced dipole moment of each molecule can be written explicitly as

$$\begin{aligned} \mu_x^{\omega} &= \alpha_{xx}^{\omega} E_{\mathrm{loc},x}^{\omega} \\ \mu_y^{\omega} &= \alpha_{yy}^{\omega} E_{\mathrm{loc},y}^{\omega} \\ \mu_z^{\omega} &= \alpha_{zz}^{\omega} E_{\mathrm{loc},z}^{\omega} \\ \mu_x^{2\omega} &= \alpha_{xx}^{2\omega} E_{\mathrm{loc},x}^{2\omega} + \beta_{xxz} E_{\mathrm{loc},x}^{\omega} E_{\mathrm{loc},z}^{\omega} + \beta_{xzx} E_{\mathrm{loc},z}^{\omega} E_{\mathrm{loc},x}^{\omega} \\ \mu_y^{2\omega} &= \alpha_{yy}^{2\omega} E_{\mathrm{loc},y}^{2\omega} + \beta_{yyz} E_{\mathrm{loc},y}^{\omega} E_{\mathrm{loc},z}^{\omega} + \beta_{yzy} E_{\mathrm{loc},z}^{\omega} E_{\mathrm{loc},y}^{\omega} \\ \mu_z^{2\omega} &= \alpha_{zz}^{2\omega} E_{\mathrm{loc},z}^{2\omega} + \beta_{zxx} E_{\mathrm{loc},x}^{\omega} E_{\mathrm{loc},x}^{\omega} + \beta_{zyy} E_{\mathrm{loc},y}^{\omega} E_{\mathrm{loc},y}^{\omega} + \beta_{zzz} E_{\mathrm{loc},z}^{\omega} E_{\mathrm{loc},z}^{\omega}. \end{aligned} \tag{3}$$

3.2. *Local field factors of the monolayer*

Now, in order to calculate these induced dipoles of the monolayer, the knowledge of the local fields $\vec{E}_{\mathrm{loc}}^{\omega}$ and $\vec{E}_{\mathrm{loc}}^{2\omega}$ at the interface needs to be described.

When an optical field is incident on a molecular monolayer at the interface between two bulk phases with dielectric constant $\varepsilon_1 = n_1^2$ and $\varepsilon_2 = n_2^2$, the induced dipole in the monolayer and the image induced dipole in the substrate all add to the local field at each individual molecule within the monolayer. Therefore the total local field is different from the applied electric field. Then [59,93,94],

$$\vec{E}_{\mathrm{loc}}(\vec{r}) = \vec{E}(\vec{r}) + \vec{E}_{\mathrm{dip}}(\vec{r}) + \vec{E}_{\mathrm{dip},I}(\vec{r}). \tag{4}$$

Here, let $\vec{r}$ be the position vector within the monolayer from the centre of the molecule at the position of the origin. Then $\vec{E}_{\mathrm{loc}}(\vec{r})$ is the local field at $\vec{r}$, and it is the sum of three contributions. Among them, $\vec{E}(\vec{r})$ is the applied field, $\vec{E}_{\mathrm{dip}}(\vec{r})$ is the field acted at this point from all the induced dipoles except the one at $\vec{r}$, and $\vec{E}_{\mathrm{dip},I}(\vec{r})$ is the field created by all the image-induced dipoles at $\vec{r}$.

Here the term $\vec{E}(\vec{r})$ is discussed first. In this case, a field of a plane wave at frequency ω is incident at an angle of α_i upon the interface from one bulk phase and reflected from the interface. Because the applied field does not have frequency 2ω, one always has $\vec{E}(\vec{r}, 2\omega) = 0$. For $\vec{E}(\vec{r}, \omega)$, because of the existence of the interface, the applied electric field is the superposition of the incident field plus the field reflected from the interface [59,93,94]. According to the Fresnel formulae [56], the total applied field $\vec{E}(\vec{r}, \omega)$ (E_x, E_y, E_z) can be determined from the incident electric field $\vec{E}_0(E_{0,x}, E_{0,y}, E_{0,z}) = E_0\hat{e}$ as follows:

$$\begin{aligned}
E_x &= \left(1 - r_p e^{i2k_1 d\cos\Omega_i}\right)E_{x,0} = \left(1 + \frac{n_1\cos\Omega_t - n_2\cos\Omega_i}{n_2\cos\Omega_i + n_1\cos\Omega_t} e^{i2k_1 d\cos\Omega_i}\right)E_{x,0} = L'_{xx}E_{x,0} \\
E_y &= \left(1 + r_s e^{i2k_1 d\cos\Omega_i}\right)E_{y,0} = \left(1 + \frac{n_1\cos\Omega_i - n_2\cos\Omega_t}{n_1\cos\Omega_i + n_2\cos\Omega_t} e^{i2k_1 d\cos\Omega_i}\right)E_{y,0} = L'_{yy}E_{y,0} \\
E_z &= \left(1 + r_p e^{i2k_1 d\cos\Omega_i}\right)E_{z,0} = \left(1 + \frac{n_2\cos\Omega_i - n_1\cos\Omega_t}{n_2\cos\Omega_i + n_1\cos\Omega_t} e^{i2k_1 d\cos\Omega_i}\right)E_{z,0} = L'_{zz}E_{z,0}.
\end{aligned} \tag{5}$$

This may be simplified as $\vec{E} = [L' \cdot \hat{e}\,]E_0$. Here, Ω_i and Ω_t are the incident angle and the refraction angle at the interface. k_1 is the wavevector in the first bulk phase, and d is the distance of the dipole from the interface. Generally for the monolayer $d \ll \lambda$, $e^{i2k_1 d\cos\Omega_i} \sim 1$. In this case, the expression of the Fresnel factor L'_{ii} is simplified to L_{ii}, which will be expressed in Section 4.

The expression of $\vec{E}(\vec{r})$ in Equation (5) is independent of the structure of the interfacial monolayer for any interface between two isotropic bulk phases. However, the expressions of the other two terms in Equation (4) depend on the model of the monolayer structure. In order to evaluate them, a square lattice model is used to represent the molecular monolayer. Other kinds of lattice models, such as the hexagonal lattice model, can also be employed and they shall generate similar results [95,96]. Here we only discuss the case using the square lattice model.

Bagchi *et al.* [93,94] and Ye *et al.* [59] used the classical discrete square point-dipole model to discuss the linear and nonlinear optical responses of the molecular monolayer, respectively. Such a square lattice model is illustrated in Figure 1. The dipoles at the interface form a two-dimensional square lattice with lattice constant a. The two bulk phases occupy the two semi-infinite spaces of $z \geq 0$ and $z \leq 0$, respectively, and they are characterized by the bulk dielectric constants ϵ_1 and ϵ_2 (the substrate), respectively. The tilt angle of the dipole with the surface normal is θ and its azimuthal orientation angle is

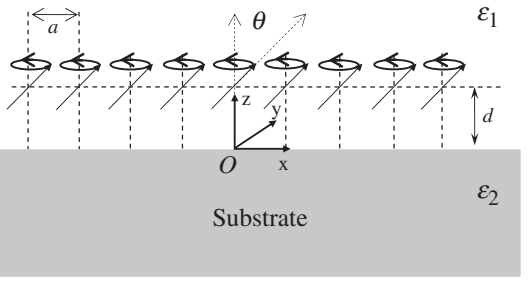

Figure 1. Illustration of an infinite lattice of point induced dipoles on a substrate interface. a is the distance between the nearest molecules, or the lattice constant; d is the distance from the centre of the point dipole to the surface of the substrate; θ is the tilt angle of the point dipoles.

randomly distributed in the plane of the interface. The distance of the point dipole to the lower substrate surface is d. The coordinates of each point dipole is then $\vec{R}_{m,n} = (ma, na, d)$, where m and n are integer indexes along the x- and y-directions from the origin $O(0,0,0)$ in the plane of the monolayer, respectively.

The contribution to the dipolar field $\vec{E}_{\text{dip}}(\vec{r})$ at an adsorbed dipole comes from the neighbouring induced dipoles within the monolayer [94]. As in previous treatments [59,93,94], the near field approximation of the local field is employed. In the near field approximation, the magnetic part of the electromagnetic field is ignored, and the retardation effects are discarded [84,93,94]. This assumption is justified because the wavelength λ of the incident electric field is much larger than the lattice constant a. Following the work of Bagchi, the electric field at the lattice point $R_{00}(0,0,d)$ which is created by the rest of the induced dipoles in the lattice plane is [93,94]

$$E_{\text{dip}}^{R_{00}} = {\sum_{m,n=-\infty}^{\infty}}' \frac{3\left[\vec{\mu}\cdot(\vec{R}_{mn}-\vec{R}_{00})\right](\vec{R}_{mn}-\vec{R}_{00}) - \vec{\mu}(\vec{R}_{mn}-\vec{R}_{00})^2}{(\vec{R}_{mn}-\vec{R}_{00})^5}$$
$$= \hat{z}\left(\frac{\mu_z}{a^3}\right)\xi_0 - \left[\hat{x}\left(\frac{\mu_x}{a^3}\right) + \hat{y}\left(\frac{\mu_y}{a^3}\right)\right]\frac{\xi_0}{2}. \quad (6)$$

The CGS unit system is used in this paper, as in many textbooks. Here μ_i are the components of the induced dipole $\vec{\mu}$. $\hat{x}$, $\hat{y}$, and $\hat{z}$ are unit vectors in laboratory coordinates. As shown in Figure 1, here the xy-plane is the plane of the substrate interface and the z-axis is along the interface normal. The prime symbol $'$ denotes that the summation does not include the origin R_{00}. The constant ξ_0 was evaluated by Topping in 1927 [96]:

$$\xi_0 = -{\sum_{m,n=-\infty}^{\infty}}' (m^2+n^2)^{-\frac{3}{2}} = -9.0336. \quad (7)$$

In Equation (6), only the induced dipole in the same plane of the interface lattice is considered. To be more rigorous, molecular layers other than the interface lattice plane also need to be considered. These layers may be the molecules or atoms of the two bulk phases, whose polarizabilities differ from those of the dipoles in the interfacial layers. Phenomenologically, let us define a vertical lattice index l and lattice constant d, with $l=0$ for the plane of the monolayer rather than the plane with origin $O(0,0,0)$. Then the total

$\vec{E}_{\rm dip}(\vec{r}) = E_{\rm dip}^{R_{00}} + E_{\rm dip}^{R_{00},\, l\neq 0}$, with $E_{\rm dip}^{R_{00},\, l\neq 0}$ as the induced dipole interaction contribution to the $R_{00}^0 = R_{00}$ origin point from the induced dipoles other than the interface lattice plane:

$$E_{\rm dip}^{R_{00},\, l\neq 0} = \sum_{l=-\infty}^{\infty}{}' \sum_{m,n=-\infty}^{\infty} \frac{3\left[\vec{\mu}^l \cdot (\vec{R}_{mn}^l - \vec{R}_{00}^0)\right](\vec{R}_{mn}^l - \vec{R}_{00}^0) - \vec{\mu}^l(\vec{R}_{mn}^0 - \vec{R}_{00}^0)^2}{(\vec{R}_{mn}^l - \vec{R}_{00}^0)^5}$$
$$= \sum_{l=-\infty}^{\infty}{}' \left(\hat{z}\left(\frac{\mu_z^l}{a_l^3}\right)\xi_0^l - \left[\hat{x}\left(\frac{\mu_x^l}{a_l^3}\right) + \hat{y}\left(\frac{\mu_y^l}{a_l^3}\right)\right]\frac{\xi_0^l}{2}\right). \tag{8}$$

Here a_l is the lattice constant of the l layer. The expression here is similar to the expressions for the image dipole term by Bagchi, Ye *et al.* [59,93,94]. Here ξ_0^l can be directly derived from Equation (6):

$$\xi_0^l = \sum_{m,n=-\infty}^{\infty} \frac{3(2ld/a_l)^2 - \left[m^2 + n^2 + (2ld/a_l)^2\right]}{\left[m^2 + n^2 + (2ld/a_l)^2\right]^{5/2}}. \tag{9}$$

Here the convergence of ξ_0^l needs to be discussed. When $ld \ll a$, we shall have $\xi_0^l \to 0$. This indicates that when the lateral separation is much larger than the separation between the two layers, the contribution from the neighbouring layers is simply negligible. For the case when d is comparable or even larger than a, to evaluate how quickly this summation converges with increase of l, Equation (9) can be converted into a more rapidly convergent series when $ld/a \gg 0$ [93,94]:

$$\xi_0^l = 16\pi^2 \sum_{m=0}^{\infty}\sum_{n=1}^{\infty} \left(m^2 + n^2\right)^{1/2} \exp\left[-4\pi l\left(\frac{\rm d}{a_l}\right)\left(m^2 + n^2\right)^{1/2}\right]. \tag{10}$$

Equation (10) indicates that ξ_0^l falls off exponentially as l increases. Generally, when $d \sim a/2$, even the contribution of the immediate neighbouring layer, i.e. $l = \pm 1$, can be neglected. This is the basis for the planewise dipole sum rule in molecular crystal theory, which shall be discussed in Section 5 [80–85].

The planewise sum rule in molecular crystal theory concluded that the contribution of the induced dipoles from neighbouring layers contribute insignificantly to the local field of the induced dipoles in the layer under consideration, compared to that from the induced dipoles in the same layer. This simple fact has significant implications. When the long chain molecules are aligned closely at the interface, the length of the molecule is usually larger than the separation between the two neighbouring molecules. Therefore, the contribution can only be from the molecular segment layer within the distance in the order of $d \sim a/2$, instead of the contribution from the whole chain of the molecule.

The image dipole contribution is just a special case of Equation (8). Bagchi *et al.* discussed and evaluated the image dipole contributions previously [59,93,94]. The image dipoles are located in the substrate at $\vec{R}'_{mn} = (ma, nb, -d)$, i.e. $l = -2$ in the general case above, and the image dipole is defined as [59,93,94]

$$\mu_I(\omega)_x = \frac{\epsilon_2 - \epsilon_1}{\epsilon_2 + \epsilon_1}(-\mu_x)$$
$$\mu_I(\omega)_y = \frac{\epsilon_2 - \epsilon_1}{\epsilon_2 + \epsilon_1}(-\mu_y) \tag{11}$$
$$\mu_I(\omega)_z = \frac{\epsilon_2 - \epsilon_1}{\epsilon_2 + \epsilon_1}(\mu_z).$$

Thus, the image dipole contribution can also be calculated with the same procedure as in Equation (8) [59,93,94]. Ye and Shen concluded that for the typical case of a metal surface, where $(\epsilon_2-\epsilon_1)/(\epsilon_2+\epsilon_1)\sim 1$, when $d\geq 2.5\,\text{Å}$ with $a=5\,\text{Å}$, the image induced dipole contribution is negligible [59]. Therefore, it is generally accepted that for the dielectric substrate, where $(\epsilon_2-\epsilon_1)/(\epsilon_2+\epsilon_1)\ll 1$, this image induced dipole term need not be considered [43–50,52,88]. Therefore, we shall neglect the image induced dipole term in the followed treatment.

It should be noted that both the $\vec{E}_{\text{dip}}(\vec{r})$ and the $\vec{E}_{\text{dip},I}(\vec{r})$ terms have the same expressions for the fundamental and second harmonic frequencies.

With all the three terms known from above, putting Equations (4), (6) and (8) into Equation (3), one has

$$\begin{aligned}
\mu_x^{\omega} &= \alpha_{xx}^{\omega} l_{xx}(\omega) E_x \\
\mu_y^{\omega} &= \alpha_{yy}^{\omega} l_{yy}(\omega) E_y \\
\mu_z^{\omega} &= \alpha_{zz}^{\omega} l_{zz}(\omega) E_z \\
\mu_x^{2\omega} &= l_{xx}(2\omega)\beta_{xxz} l_{xx}(\omega) l_{zz}(\omega) E_x^{\omega} E_z^{\omega} + l_{xx}(2\omega)\beta_{xzx} l_{zz}(\omega) l_{xx}(\omega) E_z^{\omega} E_x^{\omega} \\
\mu_y^{2\omega} &= l_{yy}(2\omega)\beta_{yyz} l_{yy}(\omega) l_{zz}(\omega) E_y^{\omega} E_z^{\omega} + l_{yy}(2\omega)\beta_{yzy} l_{zz}(\omega) l_{yy}(\omega) E_z^{\omega} E_y^{\omega} \\
\mu_z^{2\omega} &= l_{zz}(2\omega)\beta_{zxx} l_{xx}(\omega) l_{xx}(\omega) E_x^{\omega} E_x^{\omega} + l_{zz}(2\omega)\beta_{zyy} l_{yy}(\omega) l_{yy}(\omega) E_y^{\omega} E_y^{\omega} \\
&\quad + l_{zz}(2\omega)\beta_{zzz} l_{zz}(\omega) l_{zz}(\omega) E_z^{\omega} E_z^{\omega}.
\end{aligned} \tag{12}$$

Here E_i^{ω} is from Equation (5), and l_{ii} are the microscopic local field factors for the isotropic monolayer using the discrete induced dipole model. l_{ii}s are derived as below [59]:

$$\begin{aligned}
l_{xx}(\omega_i) &= \left[1+\frac{\alpha_{xx}^{\omega_i}}{2a^3}\xi_0 + \sum_{l=-\infty}^{\infty}{}' \quad \frac{\alpha_{xx}^{l,\omega_i}}{2a_l^3}\xi_0^l\right]^{-1} \\
l_{yy}(\omega_i) &= \left[1+\frac{\alpha_{yy}^{\omega_i}}{2a^3}\xi_0 + \sum_{l=-\infty}^{\infty}{}' \quad \frac{\alpha_{yy}^{l,\omega_i}}{2a_l^3}\xi_0^l\right]^{-1} \\
l_{zz}(\omega_i) &= \left[1-\frac{\alpha_{zz}^{\omega_i}}{a^3}\xi_0 - \sum_{l=-\infty}^{\infty}{}' \quad \frac{\alpha_{zz}^{l,\omega_i}}{a_l^3}\xi_0^l\right]^{-1}.
\end{aligned} \tag{13}$$

Here $\omega_i=\omega$ or 2ω, and $\alpha_{ii}^{\omega_i}$ is the linear polarizability tensor which can be calculated from the molecular polarizability values in the molecular coordinate frame $\lambda'(a,b,c)$. The summation term in Equation (13) is the dipole interaction from layers other than the interface layer, which are generally negligible. However, in Section 5, the form shall be used in the discussion of the segmentation of the chain of the molecules in the molecular monolayer. The $\xi_0=-9.0336$ is for the square lattice model as derived by Topping [96]. Since ξ_0 is negative, $l_{xx}=l_{yy}$ is generally larger than unity, while l_{zz} is smaller than unity. However, when a is small, $|\alpha_{xx}^{\omega_i}\xi_0/2a^3|>1$ can happen; this would result in negative $l_{xx}=l_{yy}$ values even under the normal dispersion condition for the bulk material. This is unique for the two-dimensional case, and no equivalent phenomena can be found for the three-dimensional case.

3.3. *Averaged linear molecular polarizability tensors of the monolayer*

The molecular polarizability at the experimental coordinates can be expressed in terms of the coordinate transformation relation: $\alpha_{ij} = \sum_{i',j'=a,b,c} R_{ii'} R_{jj'} \alpha_{i'j'}$, with $R_{\lambda,\lambda'}$ as the element of the rotational transformation matrix from the molecular coordinate system $\lambda'(a,b,c)$ to the laboratory coordinate system $\lambda(x,y,z)$ [1,97]. For an ensemble of rotationally isotropic monolayers in the xy-plane, each individual molecule possesses the same homogeneous distribution in the azimuthal orientation and the twist orientation. Then, one has

$$\begin{aligned}
\alpha_{xx} &= \frac{1}{4}\cdot\left(1+\cos^2\theta\right)\cdot\alpha_{aa} + \frac{1}{4}\cdot\left(1+\cos^2\theta\right)\cdot\alpha_{bb} + \frac{1}{2}\cdot\sin^2\theta\cdot\alpha_{cc} \\
\alpha_{yy} &= \frac{1}{4}\cdot\left(1+\cos^2\theta\right)\cdot\alpha_{aa} + \frac{1}{4}\cdot\left(1+\cos^2\theta\right)\cdot\alpha_{bb} + \frac{1}{2}\cdot\sin^2\theta\cdot\alpha_{cc} \\
\alpha_{zz} &= \frac{1}{2}\cdot\sin^2\theta\cdot\alpha_{aa} + \frac{1}{2}\cdot\sin^2\theta\cdot\alpha_{bb} + \cos^2\theta\cdot\alpha_{cc}.
\end{aligned} \tag{14}$$

Here we did not consider the case when the tilt angle θ has a distribution width. In that case, Equation (14) needs to be put into the form with ensemble average over the distribution of θ. In doing the calculations, the polarizability of the molecule or molecular groups can be obtained from many compiled sources [98–100], or from direct quantum mechanics calculations.

3.4. *Remarks on the microscopic local field factors*

The local field corrected linear and nonlinear polarizabilities in Equation (12) are the sources of the linear or nonlinear radiation from the monolayer at the interface. Their detailed expressions will not appear in the next section when we try to calculate the total radiation from the monolayer. The detailed expression in Equations (12), (13), and (14) can be used for direct calculation of the local field factors and the local field corrected polarizabilities in general.

The expression in Equation (13) can be slightly different if a non-square lattice model is assumed. For other geometries, for example, the hexagonal or equitriangular geometry, the calculation of different geometries can be put forward according to Topping's treatment [96].

Equation (13) clearly indicates that when the distance a between the neighbouring molecules in the monolayer becomes large, i.e. the submonolayer case, the l_{ii} value approaches unity very quickly. This actually defines the meaning of the word 'local', by considering how rapidly the value ξ_0 converges when doing the summation of the dipoles in the lattice plane over m and n. According to the calculations of Topping and Philpott, the convergence of the value ξ_0 is generally reached in the fourth digit before $m, n < 10$ [84,96]. For a lattice constant of $a = 5\,\text{Å}$, this means the local field calculation converges within 5 nm. Since, when a become large, the local field factors in Equation (13) decay to unity rapidly, the local field can be viewed as localized interactions within a few nanometres. The planewise sum rule also restricts the local field effect in the z-direction within only a few angstroms from the dipole under consideration. These facts provide a definition of the actual range of the local field effects within and away from the molecular plane under consideration.

By introducing the microscopic local field factors, the calculation of the response from an ensemble of induced dipoles to an electromagnetic field is reduced to the calculation of the summation of the radiation of isolated molecules or molecular dipoles interacting with the local field.

4. Coherent SHG/SFG radiation in the far field from the discrete interface induced dipoles

Here we present the calculation of the linear and second harmonic radiation in the far field according to the two-dimensional lattice of the local field corrected induced dipoles at an interface between the two isotropic bulk phases. The calculation using the square lattice model can also be performed with hexagonal or other lattice models. We shall see that since the radiation in the far field is additive for the radiating dipoles, an ensemble average treatment of the radiating dipole can be straightforwardly implemented. The following derivation uses the CGS convention, in order to be consistent with the major textbooks in the field of nonlinear optics [26,101]. Conventions to convert between the SI unit and the CGS unit systems in linear and nonlinear optics can be found in the appendices of Boyd's textbook [101].

4.1. *Radiation from a point dipole*

In this problem, the radiation from the point induced dipole $\vec{\mu}$ at the linear and second harmonic frequencies is in the upper phase (ε_1) in Figure 1. Here the origin $O(0, 0, 0)$ is at the centre of the dipole, as illustrated in Figure 2, which is different from the definition in the previous section. This is for the convenience of calculations in this section. Now, the general field radiated from an electric dipole μ along the z-direction, i.e. $\mu\hat{z}$, in the ε_1 phase is [56]

$$\begin{aligned} E_r &= \frac{2\mu k_1^3}{\varepsilon_1}\left\{\frac{1}{(k_1 r)^3} - \frac{i}{(k_1 r)^2}\right\}\cos\theta e^{i\left(\vec{k}_1\cdot\vec{r}-\omega t\right)} \\ E_\theta &= \frac{\mu k_1^3}{\varepsilon_1}\left\{\frac{1}{(k_1 r)^3} - \frac{i}{(k_1 r)^2} - \frac{1}{(k_1 r)}\right\}\sin\theta e^{i\left(\vec{k}_1\cdot\vec{r}-\omega t\right)} \\ E_\varphi &= 0. \end{aligned} \tag{15}$$

Here μ is the modulus of the induced dipole, k_1 is the wavevector in phase 1, r is the distance from the point of the dipole to the point of detection at $M(r, \theta, \varphi)$ with θ as the tilt angle and φ as the azimuthal angle in polar coordinates. If we only consider the far field, which is generally in the experimental measurements except for near-field studies, all the high order $1/r$ terms can be neglected. Therefore, only the $1/r$ term of the E_θ in Equation (15) needs to be considered.

4.2. *Phase and amplitude of the radiation in the far field from the surface dipole*

In the following, the total macroscopic radiation field at a space point $R(0, 0, R_0)$ in the reflection direction can be calculated from the summation of the field of the radiation directly from the individual induced dipole at the interface and the radiated field reflected

from the interface. In doing so, the amplitude and phase of the radiated field at $R(0, 0, R_0)$ need to be expressed as a function of the components of individual induced dipoles at the interface, before the summation can be carried out over them.

The connection between the induced-dipole components μ_x, μ_y and μ_z and their radiation field components E_x, E_y and E_z at $R(0, 0, R_0)$ is illustrated in Figure 3. The total phase at $R(0, 0, R_0)$ can be calculated by choosing the origin $O(0, 0, 0)$ as the reference point. Therefore the phase difference of the radiation field at $R(0, 0, R_0)$ between the dipole

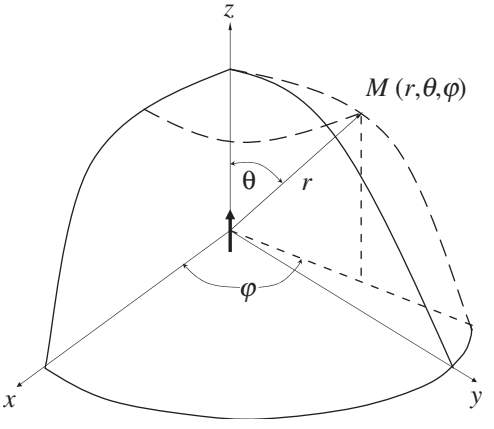

Figure 2. Polar coordinates of an electric dipole with its dipole moment vector along the z-axis. μ is the modulus of the induced dipole, r is the distance from the point of the dipole i.e. $O(0,0,0)$, to the point of $M(r, \theta, \phi)$ in the space. θ is the polar angle, and ϕ is the azimuthal angle of $M(r, \theta, \phi)$.

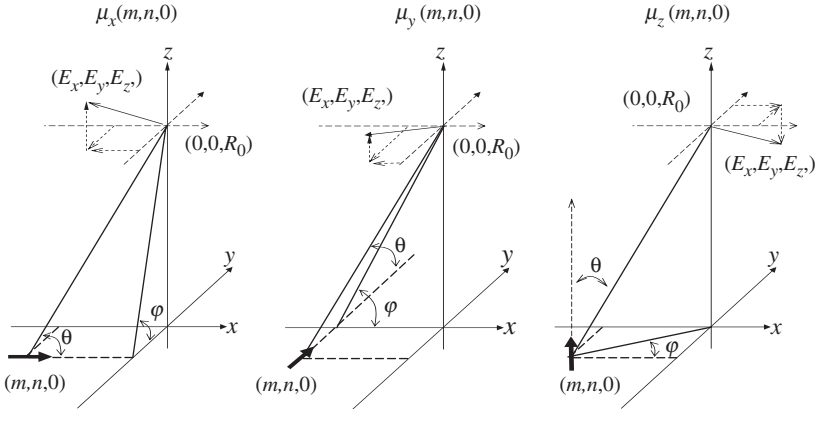

Figure 3. Definition of the coordinates system for calculation of the radiation field vector $\vec{E}(E_x, E_y, E_z)$ at the fixed space point $R(0, 0, R_0)$. The radiation field is created by the three radiating dipole components, i.e. $\mu_x(m, n, 0)$, $\mu_y(m, n, 0)$, $\mu_z(m, n, 0)$, respectively, located at the lattice point $r(m, n, 0)$. The tilt angle θ and the azimuthal angle φ are defined differently for the three dipole components as illustrated.

at the point $r(ma, na, 0)$ and the fixed origin $O(0, 0, 0)$ can be calculated from the difference of the two distances RO and Rr, i.e. $r(m, n) - R_0$, with

$$r(m,n) = \sqrt{(ma)^2 + (na)^2 + (R_0)^2}. \tag{16}$$

Now, the phase difference of the incident field at O and r on the dipole plane also needs to be calculated. When a plane wave is incident on the monolayer at the incident angle Ω_i, remembering that the incident plane is xz, and m is along the x-direction, this phase difference is $k_1^{in}(ma \sin \Omega_i)$. For the case of second harmonic generation, this phase difference involves two incoming waves, therefore the total phase difference is $2k_1^{in}(ma \sin \Omega_i)$.

Therefore, the total phase at the space point $R(0, 0, R_0)$ is the sum of all these phase differences. If we define this total phase of the radiation from the induced dipole at $r(ma, na, 0)$ to the fixed space point $R(0, 0, R_0)$, as $k_1 f(m, n)$, one has

$$f(m,n) = \sqrt{(ma)^2 + (na)^2 + (R_0)^2} + \frac{\eta k_1^{in}}{k_1}(ma \sin \Omega_i). \tag{17}$$

Here, when the radiation frequency is the same as the incoming frequency ω, then $\eta = 1$, and $k_1^{in} = k_1$; while when the radiation frequency is 2ω, then $\eta = 2$, and $k_1^{in} \neq k_1$. More generally, for the case of sum frequency generation ($\omega_3 = \omega_1 + \omega_2$), the expression for the second term in $f(m, n)$ becomes

$$\frac{ma}{k_1(\omega_3)}[k_1^{in}(\omega_1) \sin \Omega_i^{\omega_1} + k_1^{in}(\omega_2) \sin \Omega_i^{\omega_2}]. \tag{18}$$

With the phase known, the radiation field at $R(0, 0, R_0)$ generated from the dipole $\vec{\mu}(\mu_x, \mu_y, \mu_z)$ at $r(ma, na, 0)$ can be calculated separately for each μ_i according to Equation (15) with proper projection.

Then the field components E_x, E_y, E_z at $R(0, 0, R_0)$ generated by μ_x at $r(ma, na, 0)$ are

$$\begin{aligned}
E_{\mu_x,x} &= -E_{\mu_x,\theta} \sin\theta = \frac{k_1^2 \sin^2\theta}{\varepsilon_1 r(m,n)} \mu_x e^{i(k_1 f(m,n) - \omega t)} \\
E_{\mu_x,y} &= E_{\mu_x,\theta} \cos\theta \cos\varphi = -\frac{k_1^2 \sin\theta \cos\theta \cos\varphi}{\varepsilon_1 r(m,n)} \mu_x e^{i(k_1 f(m,n) - \omega t)} \\
E_{\mu_x,z} &= E_{\mu_x,\theta} \cos\theta \sin\varphi = -\frac{k_1^2 \sin\theta \cos\theta \sin\varphi}{\varepsilon_1 r(m,n)} \mu_x e^{i(k_1 f(m,n) - \omega t)}
\end{aligned} \tag{19}$$

with

$$\begin{aligned}
\sin\theta &= \frac{\sqrt{(na)^2 + R_0^2}}{\sqrt{(ma)^2 + (na)^2 + R_0^2}}, \quad \cos\theta = \frac{-ma}{\sqrt{(ma)^2 + (na)^2 + R_0^2}} \\
\sin\varphi &= \frac{R_0}{\sqrt{(na)^2 + R_0^2}}, \quad \cos\varphi = \frac{-na}{\sqrt{(na)^2 + R_0^2}}.
\end{aligned} \tag{20}$$

Similarly the field components E_x, E_y, E_z at $R(0,0,R_0)$ generated by μ_y at $r(ma,na,0)$ are

$$\begin{aligned} E_{\mu_y,x} &= E_{\mu_y,\theta}\cos\theta\cos\varphi = -\frac{k_1^2\sin\theta\cos\theta\cos\varphi}{\varepsilon_1 r(m,n)}\mu_y e^{i(k_1 f(m,n)-\omega t)} \\ E_{\mu_y,y} &= -E_{\mu_y,\theta}\sin\theta = \frac{k_1^2\sin^2\theta}{\varepsilon_1 r(m,n)}\mu_y e^{i(k_1 f(m,n)-\omega t)} \\ E_{\mu_y,z} &= E_{\mu_y,\theta}\cos\theta\sin\varphi = -\frac{k_1^2\sin\theta\cos\theta\sin\varphi}{\varepsilon_1 r(m,n)}\mu_y e^{i(k_1 f(m,n)-\omega t)} \end{aligned} \tag{21}$$

with

$$\begin{aligned} \sin\theta &= \frac{\sqrt{(ma)^2+R_0^2}}{\sqrt{(ma)^2+(na)^2+R_0^2}}, \quad \cos\theta = \frac{-na}{\sqrt{(ma)^2+(na)^2+R_0^2}} \\ \sin\varphi &= \frac{R_0}{\sqrt{(ma)^2+R_0^2}}, \quad \cos\varphi = \frac{-ma}{\sqrt{(ma)^2+R_0^2}}. \end{aligned} \tag{22}$$

Then the field components E_x, E_y, E_z at $R(0,0,R_0)$ generated by μ_z at $r(ma,na,0)$ are

$$\begin{aligned} E_{\mu_z,x} &= E_{\mu_z,\theta}\cos\theta\cos\varphi = -\frac{k_1^2\sin\theta\cos\theta\cos\varphi}{\varepsilon_1 r(m,n)}\mu_z e^{i(k_1 f(m,n)-\omega t)} \\ E_{\mu_z,y} &= E_{\mu_z,\theta}\cos\theta\sin\varphi = -\frac{k_1^2\sin\theta\cos\theta\sin\varphi}{\varepsilon_1 r(m,n)}\mu_z e^{i(k_1 f(m,n)-\omega t)} \\ E_{\mu_z,z} &= -E_{\mu_z,\theta}\sin\theta = \frac{k_1^2\sin^2\theta}{\varepsilon_1 r(m,n)}\mu_z e^{i(k_1 f(m,n)-\omega t)} \end{aligned} \tag{23}$$

with

$$\begin{aligned} \sin\theta &= \frac{\sqrt{(ma)^2+(na)^2}}{\sqrt{(ma)^2+(na)^2+R_0^2}}, \quad \cos\theta = \frac{R_0}{\sqrt{(ma)^2+(na)^2+R_0^2}} \\ \sin\varphi &= \frac{-na}{\sqrt{(ma)^2+(na)^2}}, \quad \cos\varphi = \frac{-ma}{\sqrt{(ma)^2+(na)^2}}. \end{aligned} \tag{24}$$

It is to be noted that the two angles θ and φ are not real variables in the above expressions. They are defined differently as in Figure 3 for each lattice dipole component in order to simplify the expressions above. The real variables that will be used in the following calculations are the lattice coordinates ma and na.

4.3. *Radiation field summation over the two-dimensional lattice with the principle of the stationary phase*

Now the total radiation field at $R(0,0,R_0)$ generated by the whole monolayer at the interface is the summation over the whole lattice plane $m(-\infty,+\infty)$ and $n\ (-\infty,+\infty)$:

$$\begin{aligned} E_x &= \sum_{m=-\infty}^{\infty}\sum_{n=-\infty}^{\infty}\left(E_{\mu_x,x}+E_{\mu_y,x}+E_{\mu_z,x}\right) \\ E_y &= \sum_{m=-\infty}^{\infty}\sum_{n=-\infty}^{\infty}\left(E_{\mu_x,y}+E_{\mu_y,y}+E_{\mu_z,y}\right) \\ E_z &= \sum_{m=-\infty}^{\infty}\sum_{n=-\infty}^{\infty}\left(E_{\mu_x,z}+E_{\mu_y,z}+E_{\mu_z,z}\right). \end{aligned} \tag{25}$$

The summation in Equation (25) for the total radiation field is in principle the discrete form of the integro-differential equation in molecular optics [55,56]. The asymptotic result of this summation can be evaluated by employing the condition of the far field. Because R_0 is very large as compared with the lattice constant a and the wavelength λ, the discrete summations in Equation (25) are asymptotic to a continuous integration over the variable set $(x,y)=(ma,na)$. In addition, because R_0 is large and so the phase factor $k_1 f(m,n)$ is large, the exponential factors in Equations (19), (21) and (23) oscillate very rapidly and change their signs many times as the point $r(ma,na,0)$ explores the domain of integration [56]. Under these conditions, an asymptotic value of the total electric field (E_x,E_y,E_z) at point $R(0,0,R_0)$ can be obtained with the application of the following formula, which is derived from the principle of stationary phase. The details of the stationary phase method can be found in the classic textbook by Born and Wolf [56].

Here by defining the variables $x=ma$ and $y=na$ with the lattice constant a as a very small quantity compared to the infinite size of the lattice plane, each term in the summation as shown in Equation (25) becomes the following integral and this integral is then asymptotic to the summation of the stationary phase terms as below:

$$\frac{1}{a^2}\int_{-\infty}^{\infty}\int_{-\infty}^{\infty} g(x,y)e^{ik_1 f(x,y)}\,\mathrm{d}x\,\mathrm{d}y = \frac{2\pi i}{k_1 a^2}\sum_j \frac{\sigma_j}{\sqrt{\left|\alpha_j\beta_j-\gamma_j^2\right|}} g\left(x_j,y_j\right)e^{ik_1 f\left(x_j,y_j\right)}. \tag{26}$$

Here $g(x,y)$ are the pre-exponential factors in Equations (19), (21) and (23). (x_j,y_j) are the points in the whole integration domain at which f is stationary, i.e.

$$\frac{\partial f}{\partial x}=\frac{\partial f}{\partial y}=0. \tag{27}$$

The definition of the other terms are the following:

$$\alpha_j=\left(\frac{\partial^2 f}{\partial x^2}\right)_{x_j,y_j},\ \beta_j=\left(\frac{\partial^2 f}{\partial y^2}\right)_{x_j,y_j},\ \gamma_j=\left(\frac{\partial^2 f}{\partial x\partial y}\right)_{x_j,y_j} \tag{28}$$

and

$$\sigma_j = \begin{cases} +1 & \text{if } \alpha_j\beta_j > \gamma_j^2,\ \alpha_j > 0, \\ -1 & \text{if } \alpha_j\beta_j > \gamma_j^2,\ \alpha_j < 0, \\ -i & \text{if } \alpha_j\beta_j < \gamma_j^2. \end{cases} \tag{29}$$

Using the stationary phase condition in Equation (27) and the expression for f in Equation (17), a single stationary point (x_1, y_1) is obtained, and

$$x_1 = -R_0 \tan\Omega,\ y_1 = 0. \tag{30}$$

Here $\Omega = \Omega_i$ is the direct result of the stationary phase condition for the linear radiation, and for the second harmonic radiation Ω to satisfy the relationship $k_1(2\omega)\sin\Omega = 2k_1^{in}(\omega)\sin\Omega_i$. Similarly, one can also show explicitly that for the sum frequency radiation, Ω has to satisfy the relationship $k_1(\omega_3)\sin\Omega = k_1^{in}(\omega_1)\sin\Omega_i^{\omega_1} + k_1^{in}(\omega_2)\sin\Omega_i^{\omega_2}$. These are just the condition for the general law of reflection in linear and nonlinear optics, as given by Bloembergen and Pershan, as derived from the Maxwell boundary conditions [35]. From these results we shall show later that at the far field space point $R(0, 0, R_0)$, the radiation field is in the direction of Ω, which satisfies the general law of reflection in linear and nonlinear optics. It is interesting that these conditions came incidentally as a solution from the molecular optics treatment. This fact further illustrates the general equivalence of the macroscopic Maxwell equations with boundary conditions and the microscopic molecular optics treatment [55,56].

Now with the stationary phase point value, we have

$$\begin{aligned} f(x_1, y_1) &= R_0\cos\Omega \\ \frac{\sigma_1}{\sqrt{|\alpha_1\beta_1 - \gamma_1^2|}} &= \frac{R_0}{\cos^2\Omega}. \end{aligned} \tag{31}$$

Here $\sigma_1 = 1$ because $\alpha_1 > 0$ and $\alpha_1\beta_1 - \gamma_1^2 > 0$. Now putting all these values into the expressions in Equation (25), we have the radiation field components at the space point $R(0, 0, R_0)$ that are directly radiated from the whole induced dipole lattice as the following:

$$\begin{aligned} E_x^{R_1} &= \frac{2\pi}{a^2\varepsilon_1} ik_1(\mu_x\cos\Omega - \mu_z\sin\Omega)e^{i(k_1R_0\cos\Omega - \omega t)} \\ E_y^{R_1} &= \frac{2\pi}{a^2\varepsilon_1} ik_1\frac{\mu_y}{\cos\Omega}e^{i(k_1R_0\cos\Omega - \omega t)} \\ E_z^{R_1} &= \frac{2\pi}{a^2\varepsilon_1} ik_1\left(-\mu_x\sin\Omega + \mu_z\frac{\sin^2\Omega}{\cos\Omega}\right)e^{i(k_1R_0\cos\Omega - \omega t)}. \end{aligned} \tag{32}$$

4.4. *Coherent SHG/SFG radiation in the far field from the induced dipole lattice*

In order to calculate the total radiated field at $R(0, 0, R_0)$, besides the direct radiation from the induced dipoles at the interface, the radiation in the forward direction which is reflected from the interface also needs to be evaluated. The above procedures can be

repeated to calculate the radiated field at the image point $R_i(0,0,-R_0)$ in the isotropic phase ε_1 from the whole induced dipole lattice. We have

$$\begin{aligned} E_x^{T_1} &= \frac{2\pi}{a^2\varepsilon_1} ik_1(\mu_x \cos\Omega + \mu_z \sin\Omega) e^{i(k_1 R_0 \cos\Omega - \omega t)} \\ E_y^{T_1} &= \frac{2\pi}{a^2\varepsilon_1} ik_1 \frac{\mu_y}{\cos\Omega} e^{i(k_1 R_0 \cos\Omega - \omega t)} \\ E_z^{T_1} &= \frac{2\pi}{a^2\varepsilon_1} ik_1 \left(\mu_x \sin\Omega + \mu_z \frac{\sin^2\Omega}{\cos\Omega}\right) e^{i(k_1 R_0 \cos\Omega - \omega t)}. \end{aligned} \tag{33}$$

Because the choice of the space point $R(0,0,R_0)$ and $R_i(0,0,-R_0)$ is rather arbitrary, and the radiation field components in Equations (32) and (33) are both directional and the amplitudes of both plane waves are independent of the value of R_0, the coherence of the radiation from the induced dipole lattice is conserved at the far field.

According to the Fresnel formulae [56], the amplitudes of the reflected electric field components are

$$\begin{aligned} E_x^{R_2} &= -r_p E_x^{T_1} = \frac{n_1 \cos\Omega_t - n_2 \cos\Omega_i}{n_2 \cos\Omega_i + n_1 \cos\Omega_t} E_x^{T_1} \\ E_y^{R_2} &= r_s E_y^{T_1} = \frac{n_1 \cos\Omega_i - n_2 \cos\Omega_t}{n_1 \cos\Omega_i + n_2 \cos\Omega_t} E_y^{T_1} \\ E_z^{R_2} &= r_p E_z^{T_1} = \frac{n_2 \cos\Omega_i - n_1 \cos\Omega_t}{n_2 \cos\Omega_i + n_1 \cos\Omega_t} E_z^{T_1}. \end{aligned} \tag{34}$$

The phase difference between the direct radiation field and the reflected field is determined by the distance between the dipole layer and the interface d and the radiation angle Ω as $2k_1 d \cos\Omega$. Therefore the total radiation field at $R(0,0,R_0)$ is the phase shifted sum of the E^{R_1} and E^{R_2} fields in Equations (32) and (34). We have

$$\begin{aligned} E_{x,\text{total}} &= \frac{2\pi}{a^2\varepsilon_1} ik_1 \left(\mu_x \cos\Omega - \mu_z \sin\Omega - r_{2p}(\mu_x \cos\Omega + \mu_z \sin\Omega) e^{i2k_1 d\cos\Omega}\right) e^{i(k_1 R_0 \cos\Omega - \omega t)} \\ &= \frac{2\pi}{a^2\varepsilon_1} ik_1 \left(\cos\Omega L'_{xx}\mu_x - \sin\Omega L'_{zz}\mu_z\right) e^{i(k_1 R_0 \cos\Omega - \omega t)} \\ E_{y,\text{total}} &= \frac{2\pi}{a^2\varepsilon_1} ik_1 \left(\frac{\mu_y}{\cos\Omega} + r_{2s}\frac{\mu_y}{\cos\Omega} e^{i2k_1 d\cos\Omega}\right) e^{i(k_1 R_0 \cos\Omega - \omega t)} \\ &= \frac{2\pi}{a^2\varepsilon_1} ik_1 \left(\frac{1}{\cos\Omega} L'_{zz}\mu_y\right) e^{i(k_1 R_0 \cos\Omega - \omega t)} \\ E_{z,\text{total}} &= \frac{2\pi}{a^2\varepsilon_1} ik_1 \left(-\mu_x \sin\Omega + \mu_z \frac{\sin^2\Omega}{\cos\Omega} + r_{2s}\left(\mu_x \sin\Omega + \mu_z \frac{\sin^2\Omega}{\cos\Omega}\right) e^{i2k_1 d\cos\Omega}\right) e^{i(k_1 R_0 \cos\Omega - \omega t)} \\ &= \frac{2\pi}{a^2\varepsilon_1} ik_1 \left(-\sin\Omega L'_{xx}\mu_x + \frac{\sin^2\Omega}{\cos\Omega} L'_{zz}\mu_z\right) e^{i(k_1 R_0 \cos\Omega - \omega t)}. \end{aligned} \tag{35}$$

Here the induced dipole components μ_x, μ_y, and μ_z are as defined in Equation (12), and the L'_{ii} are as defined in Equation (5). Considering the fact that the thickness of the

monolayer is generally much smaller than the magnitude of the optical wavelength, i.e. $d \ll \lambda$, the phase factor $e^{i2k_1 d\cos\Omega} \to 1$. Therefore, L'_{ii} becomes

$$\begin{aligned} L_{xx} &= \frac{2n_1\cos\Omega_t}{n_2\cos\Omega_i + n_1\cos\Omega_t} = \frac{2\varepsilon_1 k_{2z}}{\varepsilon_2 k_{1z} + \varepsilon_1 k_{2z}} \\ L_{yy} &= \frac{2n_1\cos\Omega_i}{n_1\cos\Omega_i + n_2\cos\Omega_t} = \frac{2k_{1z}}{k_{1z} + k_{2z}} \\ L_{zz} &= \frac{2n_2\cos\Omega_i}{n_2\cos\Omega_i + n_1\cos\Omega_t} = \frac{2\varepsilon_2 k_{1z}}{\varepsilon_2 k_{1z} + \varepsilon_1 k_{2z}}. \end{aligned} \tag{36}$$

These expressions differ from the expression given by Wei *et al.* [42] in the L_{zz} term by a factor of ε_1. In most cases, the upper phase is either vacuum or air, therefore $\varepsilon_1 = 1$ and there is no influence on the actual L_{zz} value. However, when $\varepsilon_1 \neq 1$ as for the buried interface, such a difference can be significant. The L_{zz} expression given by Wei *et al.* [42] was the result with a three-layer model when the middle phase, i.e. the interface layer, is considered a thin but macroscopic layer. As discussed in Section 5.1, such a three-layer assumption is physically inappropriate for the submonolayer and monolayer cases.

These L_{ii} values are clearly the results for the two-phase model. This indicates explicitly that when dealing with the macroscopic electric field at the interface, the existence of the interfacial molecular monolayer or submonolayer has no influence on the macroscopic field, as long as the microscopic local field effect has been considered. Therefore, the problem of the linear macroscopic dielectric constant for the interface layer is not a issue in this treatment. This shall be discussed in detail in Section 5.1.

Now the radiation field components in the second harmonic frequency are

$$\begin{aligned} E_x^{2\omega} &= \frac{2\pi}{a^2\varepsilon_1(2\omega)} ik_1^{2\omega}\left(\cos\Omega_{2\omega} L_{xx}^{2\omega}\mu_x^{2\omega} - \sin\Omega_{2\omega} L_{zz}^{2\omega}\mu_z^{2\omega}\right) e^{i(k_1^{2\omega}R_0\cos\Omega_{2\omega} - 2\omega t)} \\ E_y^{2\omega} &= \frac{2\pi}{a^2\varepsilon_1(2\omega)} ik_1^{2\omega}\left(\frac{1}{\cos\Omega_{2\omega}} L_{zz}^{2\omega}\mu_y^{2\omega}\right) e^{i(k_1^{2\omega}R_0\cos\Omega_{2\omega} - 2\omega t)} \\ E_z^{2\omega} &= \frac{2\pi}{a^2\varepsilon_1(2\omega)} ik_1^{2\omega}\left(-\sin\Omega_{2\omega} L_{xx}^{2\omega}\mu_x^{2\omega} + \frac{\sin^2\Omega_{2\omega}}{\cos\Omega_{2\omega}} L_{zz}^{2\omega}\mu_z^{2\omega}\right) e^{i(k_1^{2\omega}R_0\cos\Omega_{2\omega} - 2\omega t)}. \end{aligned} \tag{37}$$

Here $k_1^{2\omega} = 2\omega\sqrt{\varepsilon_1(2\omega)}/c$, where c is the velocity of light in vacuum. Now with the second harmonic field components determined, the intensity of the SH field can be directly calculated by the magnitude of the time averaged Poynting vector as defined below [101]:

$$I(\omega) = \frac{c}{2\pi}\sqrt{\varepsilon_1(\omega)}\left|E_i(\omega)\right|^2. \tag{38}$$

Then put the expressions in Equations (37) and (12) into Equation (38), and after taking care of the proper projection coefficients of the fundamental and second harmonic electric fields, we have

$$I(2\omega) = \frac{32\pi^3\omega^2\sec^2\Omega_{2\omega}}{c^3[\epsilon_1(2\omega)]^{1/2}\epsilon_1(\omega)}\left|\chi_{\text{eff}}(2\omega)\right|^2 I^2(\omega) \tag{39}$$

$$\chi_{\text{eff}} = [L(2\omega)\cdot\hat{e}(2\omega)]\cdot\chi(2\omega) : [L(\omega)\cdot\hat{e}(\omega)][L(\omega)\cdot\hat{e}(\omega)]. \tag{40}$$

Here $I(\omega)$ is the intensity of the incident laser beam as defined in Equation (38), and $\Omega_{2\omega}$ is the outgoing angle of the second harmonic radiation from the surface normal. $\epsilon_1(\omega)$ and $\epsilon_1(2\omega)$ are the bulk dielectric constants of the upper bulk phase at the frequency ω and 2ω, respectively. $\hat{e}(2\omega)$ and $\hat{e}(\omega)$ are the unit vectors of the electric field at 2ω and ω, respectively. $L(2\omega)$ and $L(\omega)$ are the tensorial Fresnel factors for 2ω and ω, respectively, as defined in Equation (36). The scalar property $\chi_{\text{eff}}(2\omega)$ is the effective macroscopic second-order susceptibility of the interface. The $\chi(2\omega)$ represents the area-averaged macroscopic second harmonic susceptibility tensors defined as $\chi_{ijk}(2\omega) = l_{ii}(2\omega)l_{jj}(\omega)l_{kk}(\omega)\beta_{ijk}/a^2 = N_s l_{ii}(2\omega)l_{jj}(\omega)l_{kk}(\omega)\langle\beta_{i'j'k'}\rangle$, with a as the lattice constant, N_s as the surface number density, and $\langle\,\rangle$ represents ensemble average over different orientational distributions.

Even though the treatment here is based on the discrete lattice model and molecular optics treatment, as expected the expressions in Equations (37) and (39) are exactly the same as those in the previous treatment by Heinz and Shen for the infinitesimally thin nonlinear polarization sheet using the Maxwell equations and boundary conditions [6,34,54,57,58]. This indicates that the treatment with the square point-dipole lattice model together with a molecular optics approach presented here is correct.

It can be shown accordingly that for the SFG from the interface,

$$I(\omega_{\text{SF}}) = \frac{8\pi^3\omega^2 \sec^2 \Omega_{\text{SF}}}{c^3[\epsilon_1(\omega_{\text{SF}})\epsilon_1(\omega_1)\epsilon_1(\omega_2)]^{1/2}} \left|\chi_{\text{eff}}(\omega_{\text{SF}})\right|^2 I(\omega_1)I(\omega_2) \tag{41}$$

$$\chi_{\text{eff}} = [L(\omega_{\text{SF}}) \cdot \hat{e}(\omega_{\text{SF}})] \cdot \chi(\omega_{\text{SF}}) : [L(\omega_1) \cdot \hat{e}(\omega_1)][L(\omega_2) \cdot \hat{e}(\omega_2)]. \tag{42}$$

4.5. *Remarks on the microscopic SHG/SFG theory*

The following points need to be further illustrated for the formulae derived above.

(a) The expressions in Equations (37) and (39) were obtained through the square induced dipole lattice model. Using other types of plane lattice model can also give the same asymptomatic expressions at the far field, except that the area-averaged macroscopic second harmonic susceptibility tensors may take slightly different expressions. The near field results would be different for different lattice models, because generally no analytical asymptomatic results can be reached for the near field case. In other words, the molecular optics approach described here can also be used to treat the near field cases; this is a clear advantage of the molecular optics approach.

(b) Here the area-averaged macroscopic second harmonic susceptibility tensors $\chi_{ijk}(2\omega)$ and the factor $1/a^2$ in Equation (37) needs to be discussed. a^2 is the average area per induced dipole in the lattice plane under the square induced-dipole lattice model. It comes into the expression naturally because of the summation, or integration, over the whole lattice plane. Therefore, μ_i/a^2 is the area averaged induced dipole, and $\chi_{ijk}(2\omega)$ is the area-averaged macroscopic second harmonic susceptibility tensor. In the previous macroscopic treatments on second harmonic generation [6,57], an infinitesimally thin polarization sheet

layer was used, and the polarization for this interface layer was defined in the form of $P(2\omega) = \chi(2\omega)\delta(z) : E(\omega)E(\omega)$, or sometimes $P(2\omega) = \chi(2\omega) : E(\omega)E(\omega)$, and then put into the Maxwell equations [6,26,57,102]. In this way, it is confusing when making the dimensional analysis of the formulae when trying to apply the interface polarization term in the Maxwell equations. However, in the microscopic molecular optics treatment, there is no ambiguity in this case, and the $\chi(2\omega)$ tensor has to have the dimension of an area-averaged second order nonlinear polarizability.

(c) The ensemble average of the $\chi_{ijk}(2\omega)$ tensors. In the calculation of the summation and its asymptomatic results in the far field, the actual size of the lattice constant a can be treated arbitrarily as long as the lattice constant a is microscopic, i.e. much smaller than the optical wavelength. Because the total radiation is additive as in Equation (25), even though the surface is not a square lattice for each individual dipole, one can always divide the surface layer into the square lattice with microscopic unit cells each containing a group of individual neighbouring induced dipoles. Therefore, this approach actually allows making an ensemble average within each unit cell. It even allows the unit cell to contain several layers of molecules close to the interface region. This further allows the inclusion of the contributions of the quadrupolar terms, the interfacial discontinuity terms, as well as the field induced third order terms into the effective unit induced dipole cell at the interface region [6,26,31,35,102,103]. This also indicates that even for surfaces where the point-dipole model is no longer valid, the macroscopic expression should still be the same, and the surface can still be divided into unit cells and be treated as discrete microscopic nonlinear emitters. Of course, each of these different microscopic models has to be treated with different microscopic descriptions and analysed according to the symmetry properties of the area-averaged effective microscopic polarizability tensor terms χ_{ijk} of the unit cell as defined. Thus, Equations (37) and (39) are general for the second harmonic generation from the whole interface region. Now it is also possible to make a microscopic treatment or calculation with different microscopic models of the interface region. A similar treatment can be performed for the sum frequency generation process from the interface.

Here the useful general expressions of SHG from a rotationally isotropic molecular interface are summarized below. If we let α_{in} be the polarization angle of the incident electric field, let γ_{out} be the polarization angle of the second harmonic electric field, $\chi_{\text{eff},\alpha_{\text{in}}-\gamma_{\text{out}}}$ be the corresponding effective macroscopic nonlinear susceptibility, then $\chi_{\text{eff},\alpha_{\text{in}}-\gamma_{\text{out}}}$ of an achiral interface can be expressed as linear combinations of the three independently measurable terms with the following polarization combinations: s_{in}-p_{out}, 45°_{in}-s_{out}, p_{in}-p_{out}, with s as the polarization perpendicular to the incident plane, and p as the polarization in the incident plane. Let Ω_{ω} and $\Omega_{2\omega}$ be the incoming and outgoing angles, respectively. One has [2]

$$\chi_{\text{eff},\alpha_{\text{in}}-\gamma_{\text{out}}} = \chi_{\text{eff},45^{\circ}-s} \sin 2\alpha \sin\gamma + \left[\chi_{\text{eff},s-p} \sin^2\alpha + \chi_{\text{eff},p-p} \cos^2\alpha\right] \cos\gamma \qquad (43)$$

with

$$\begin{aligned}
\chi_{\text{eff},\,s-p} &= L_{zz}(2\omega)L_{yy}(\omega)L_{yy}(\omega)\sin\Omega_{2\omega}\chi_{zyy} \\
\chi_{\text{eff},\,45^\circ-s} &= L_{yy}(2\omega)L_{zz}(\omega)L_{yy}(\omega)\sin\Omega_{\omega}\chi_{yzy} \\
\chi_{\text{eff},\,p-p} &= -2L_{xx}(2\omega)L_{zz}(\omega)L_{xx}(\omega)\cos\Omega_{2\omega}\sin\Omega_{\omega}\cos\Omega_{\omega}\chi_{xzx} \\
&\quad + L_{zz}(2\omega)L_{xx}(\omega)L_{xx}(\omega)\sin\Omega_{2\omega}\cos^2\Omega_{\omega}\chi_{zxx} \\
&\quad + L_{zz}(2\omega)L_{zz}(\omega)L_{zz}(\omega)\sin\Omega_{2\omega}\sin^2\Omega_{\omega}\chi_{zzz}.
\end{aligned} \tag{44}$$

For a chiral interface, an additional term $\chi_{\text{eff,chiral}}$ has to be included with the non-zero chiral susceptibilities, i.e. $\chi_{xyz}=\chi_{xzy}=-\chi_{yzx}=-\chi_{yxz}$ [104]. One has,

$$\begin{aligned}
\chi_{\text{eff},\,\alpha_{\text{in}}-\gamma_{\text{out}}} &= \left[\chi_{\text{eff},\,45^\circ-s}\sin 2\alpha + \chi_{\text{eff, chiral}}\cos^2\alpha\right]\sin\gamma \\
&\quad + \left[\chi_{\text{eff},\,s-p}\sin^2\alpha + \chi_{\text{eff},\,p-p}\cos^2\alpha + \chi_{\text{eff, chiral}}\sin 2\alpha\right]\cos\gamma
\end{aligned} \tag{45}$$

with

$$\chi_{\text{eff, chiral}} = 2L_{xx}(2\omega)L_{yy}(\omega)L_{zz}(\omega)\sin\Omega_{\omega}\cos\Omega_{\omega}\chi_{xyz}. \tag{46}$$

Details of the quantitative experimental measurement and interpretation of the interface SHG, as well as the SFG-vibrational spectroscopy, of molecular interfaces with these formulations can be found in the recent literature [1,2].

5. Evaluation of the local field factors in the quantitative SHG/SFG spectroscopy

Two of the central issues with general interests in the quantitative interpretation of the SHG and SFG-VS data are whether the molecular monolayer has a linear macroscopic dielectric constant and how the microscopic local field effects is evaluated. Many researchers already provided most of the answers as reviewed in the Introduction above, and we are trying to present a coherent picture here with the formulation above. Based on the microscopic treatment of the SHG and SFG-VS from the molecular interface, these issues are to be discussed.

5.1. *Disappearance of the linear macroscopic dielectric constant of the molecular monolayer or submonolayer*

Concern for the linear macroscopic dielectric constant of the interface stems from the beginning of the development of SHG and SFG-VS as quantitative surface spectroscopic probes [26]. These insights and discussion led to the later treatment by Shen to replace the macroscopic dielectric constant of the interface layer in the early treatment [26,34,57] with microscopic local field factors [42,54,59]. Here the rigorous molecular optics treatment in Sections 3 and 4 with the discrete induced dipole lattice model can provide a solid foundation for this approach.

According to the microscopic molecular optics treatment, the linear macroscopic dielectric constant of the monolayer or submonolayer is no longer an issue as described in the detailed derivations in Sections 3 and 4.

(a) Firstly, we consider a few nonlinear induced dipoles situated at the interface between the two isotropic bulk phases, for example, the vacuum–metal or the fluid–solid interfaces. The interface induced dipoles are situated in the vacuum phase and they do not even form an interface layer. Therefore, under the submonolayer condition up to a full monolayer condition, the treatment as presented in Sections 3 and 4 with the discrete induced dipole lattice model is rigorous, and no linear macroscopic dielectric constant can be invoked for the molecular layer. When this is validated, then consider the case that there is an additional submonolayer up to a full monolayer on top of the first full monolayer at the air–metal interface. The treatment of this top layer must be the same, i.e. no need to invoke a linear macroscopic dielectric constant for this top layer, and only the microscopic local field effect, i.e. the dipole screening effect, need be considered [59,93]. Since the interface layer in between any two isotropic bulk phases is usually one or a few molecular monolayers thick, the discrete induced dipole lattice model must be a generally realistic treatment of the interface problem. In simple words, this implies that there is no need to invoke the linear macroscopic dielectric constant for the interface consisting of a few molecular layers.

(b) Secondly, let us consider the case of submonolayer adsorption of organic molecules at the air–liquid interface, e.g. a submonolayer of surfactant molecules at the air–water interface. Since the air–water interface is known to be sharp at less than 4 Å [105–107], one can surmise that the hydrophobic part of the adsorbed molecule is in the air phase and the hydrophilic part is in the water phase. In this case, the treatment in Sections 3 and 4 with the discrete induced dipole lattice model can be used to treat the head and tail groups, respectively, especially for the SFG-VS when the tail and the head group of the interfacial surfactant molecule are probed with different vibrational frequencies. The radiation from the molecular induced dipole in phase 2 (ε_2) can be treated similarly and readily as in Sections 3 and 4. Nevertheless, in these cases, the continuous surface sheet layer model does not provide a realistic representation of the microscopic molecular picture.

In the above cases, the linear macroscopic dielectric constant of the interface layer should not be a concern for surface nonlinear optics whenever the surface contribution is dominant. Therefore, the macroscopic optical field at the interface can be well described with an explicit two-phase model, as in Equation (36). The major concern by Roy [60] on the macroscopic linear anisotropy of the interface monolayer in the SHG treatment is not a real issue, at least for the submonolayer up to the monolayer regime [26]. Nevertheless, according to the treatment presented in Sections 3 and 4, the local field effects of the induced dipoles at the interfaces need to be treated accordingly. This separation of the macroscopic and the microscopic anisotropy of the interfacial monolayer ensures the simplicity and effectiveness in the interpretation of the surface SHG and SFG-VS data.

Of course, the above discussion may not be entirely suitable for the situation when the interface consists of a large number of layers of anisotropic nonlinear induced dipoles and becomes macroscopic. However, as long as such a film is thin enough not to significantly

alter the macroscopic reflection and transmission coefficients of light from the interface between the two isotropic phases, there is no reason that one should worry about the issue of the linear macroscopic dielectric constant of the film itself [26,60].

5.2. *Planewise dipole sum rule and local field factor in the interface layer*

The treatment of the microscopic local field effect is expressed in Equation (13) in Section 3. In order to implement these formulae to correctly calculate or evaluate the local field factors in the monolayer, the planewise dipole sum rule in molecular crystal dielectric theory needs to be discussed [80–85]. The planewise dipole sum rule in studying the interface problem was discussed by Munn *et al.* in the 1990s [49,86–89]. However, its implications have not been picked up by practitioners in the SHG and SFG-VS community. These issues need to be addressed.

Let us look at the problems in the quantitative interpretation of the SHG measurement data. In their SHG studies of a self-assembled-monolayer (SAM) at a gold substrate, Eisert *et al.* carefully compared the results with the macroscopic three-layer model and the two-layer model, as well as the local field corrections. They concluded that using the two-layer model without local-field correction gave most satisfactory agreement of the molecular orientation with the results from the NEXAFS and IR spectroscopy measurements [52]. According to Eisert *et al.*, the parameters used to calculate the local field factors in Equations (13) and (14) of the pNA [O_2N–C_6H_4–] monolayer in the SHG experiment are: $a = 5$ to 5.5 Å, $\alpha_{aa} = \alpha_{bb} = 16.4\,\text{Å}^3$, $\alpha_{cc} = 27.3\,\text{Å}^3$, and $\theta \sim 52^\circ$ from NEXAFS measurement. Then, one has $\alpha_{xx} = \alpha_{yy} = 19.8\,\text{Å}^3$ and $\alpha_{zz} = 20.5\,\text{Å}^3$, then $l_{xx} = l_{yy} = 3.51$ to 2.16 and $l_{zz} = 0.403$ to 0.473. Therefore, the effective microscopic dielectric constant defined as $\varepsilon' = n'^2 = l_{yy}/l_{zz}$ becomes 8.71 to 4.57, or $n' = 2.95$ to 2.14. Here the definition $\varepsilon' = n'^2 = l_{xx}/l_{zz}$ follows the definition by Wei *et al.* [42]. These are unreasonably large values and the calculation by Eisert *et al.* concluded that in order to get $\theta \sim 52^\circ$ from the SHG data, n' has to be close to unity, i.e. neglecting the microscopic local field effect.

This conclusion by Eisert *et al.* is in direct disagreement with the formulation provided by Shen *et al.* [42]. However, the formulation with the microscopic local field factors by Shen *et al.* is validated by the treatment in this work. When the molecule is longer than their separation, the point-dipole model is no longer valid. Therefore, the premise for the formulae to calculate the local field factors provided by Shen *et al.* [42] is no longer valid. Therefore, the answer to the difficulties of Eisert *et al.* in calculating the local field factors lies in the planewise dipole sum rule [80–85]. Munn *et al.* in the 1990s started using it to tackle the problem of the overestimation of the local field factors by putting the linear polarizability of the whole molecule into Equation (13) [49,86–89].

The planewise dipole sum rule was originally developed in explaining optical and dielectric phenomena in molecular crystals, such as the long range coupling of the exciton in the molecular crystal, in the early 1970s [80–85]. It has been known that the plane sum in the summation of the dipole–dipole interaction as in Equation (6), which leads to expressions of the local field factors in Equation (13), falls off exponentially as the perpendicular distance from the plane of the origin increases [83,84]. Philpott *et al.* showed that even for strong dipoles in molecular crystals, the contribution of the immediate neighbouring layer is less than 1% of the contribution of the plane of the origin, and the

total sum of all the rest of the layers up to infinite distance, other than the plane of origin, is generally less than 10% [83,84].

When the lateral distance between molecules is smaller than the length of the molecule, there is no reason to view the molecule as a whole when calculating the local field factors using Equation (13). Munn *et al*. thus proposed a bead model to divide the interface long chain molecule into a chain of sphere beads in calculating the local field factors for each submolecular segment layer for the long chain molecules in the Langmuir–Blodgett film [49,86–89]. This bead model also unknowingly supported the calculations by Ye and Shen on the contribution of the local field factors from the image induced dipoles at a vacuum–metal interface [59]. They conclude that for $\varepsilon_{\text{metal}} = 10$, i.e. $(\varepsilon - 1)/(\varepsilon + 1) \sim 1$, when $d/a > 1/2$, the image-induced dipole contribution is negligible. Here $d/a > 1/2$ is just the sphere bead condition in Munn's treatment if the interfacial induced dipole and its image induced dipole are considered as a whole.

In our treatment, the planewise dipole sum rule is explicitly described with Equation (10). Evaluation of the ξ_0^l term indicates that in most cases, even the immediate neighbouring term, i.e. $l = \pm 1$, is often negligible when d is larger than 3 Å. This indicates that when dealing with the local field factor calculations with Equation (13), the depth of the segmentation of the molecular layer is generally no more than 3 Å. However, this number may not be correct for the big chromophores with conjugate structures, which may require quantum mechanical treatment or more complex models rather than the simple classical dipole model.

With the planewise dipole sum rule in mind, now one can understand why in the Eisert *et al*. case [52] the local field factors are overestimated compared to the actual value. Because the SAM monolayer is closely packed, if one uses the α_{ii} value of the whole pNA group, the l_{ii} factors should deviate further from unity. If one uses the sphere bead model, the l_{ii} is going to be much closer to unity. Actually, if we closely inspect the formulae in Equation (13), one can expect that when $|\alpha_{ii}\xi_0/2a^3| > 1$, then l_{xx} and l_{yy} can even become a large negative value. If the sphere bead model is not used, a closely packed long chain molecular monolayer would easily have unreasonable local field factors according to Equation (13) without considering the planewise sum rule. Therefore, the planewise dipole sum rule is very important and has to be implemented for the evaluation of the microscopic local file factors in the molecular monolayer.

One direct conclusion from the segmentation of the interfacial molecules for the implementation of this planewise dipole sum rule is that because the different groups in the same molecule have different linear polarizabilities, and because the same molecular group may have different polarizabilities at different frequencies, their local field factors can be significantly different when these groups occupy different segmented layers when the monolayer is closely packed. This immediately poses questions to the practice of using the same and simple value for the interface local field factors in SHG and SFG-VS studies [54,61,71]. One of the example is for the SHG and SFG-VS studies of the 5CT [CH_3–$(CH_2)_4$–$(C_6H_4)_3$–CN] monolayer at the air–water interface [54]. In the interpretation of the SHG measurement of the –$(C_6H_4)_3$–CN chromophore and the SFG-VS measurement of the –CH_3 and –CN groups of the 5CT monolayer, the same local field factor value, i.e. $n' = 1.18$, was used for all three molecular chromophore or groups. Close inspection shows that the orientational angle thus obtained is actually inconsistent with other studies [108–112].

Therefore, whether the same $n' = 1.18$ value is suitable for the three groups needs to be re-examined.

In a recent study in our research group, using a self-consistent approach we found that $n'(800\,\text{nm}) \sim 1.5$ and $n'(400\,\text{nm}) \sim 2.5$ for the $-(C_6H_4)_3-CN$ chromophore from the SHG data, significantly different from that of the $-CH_3$ or –CN group, and consistent with the large polarizability of the $-(C_6H_4)_3-CN$ chromophore [110,111]. The orientational angle thus obtained for the $-(C_6H_4)_3-CN$ chromophore in the closely packed Langmuir monolayer at the air–water interface is about $20^\circ \sim 30^\circ$, consistent with the orientational angle obtained in other studies [108,109].

Now, if the ε' or n' values were different, then why, in past SFG-VS studies, was it quite successful to use simple values such as $n' = 1.18$, or why use the average value of the optical constant of the two neighbouring bulk phases for molecular groups and chromophores at the common dielectric interfaces [1,2,54,61,71,112]? Here we can show that these values are actually quite reasonable approximations of the common simple molecular groups such as $-CH_3$, –C=O, etc. at the interface.

The experimental linear polarizability values of many common molecular group are as listed in Table 1 [98–100]. The values for simple organic groups are typically in the range 1.5–3.0 Å^3. Considering that the segmentation depth is expected to be no more than 3 Å for simple molecules with no big chromophores with conjugated structure, as a realistic approximation, the typical α value used in the calculation is set in between 2 and 4 Å^3. Considering the fact that at the molecular interface a typical molecular group per area is about 20 Å^2 (square lattice constant $a \sim 4.5$ Å) to 30 Å^2 ($a \sim 5.5$ Å), the simulations in Table 2 shown that the typical ε' values for these groups are 1.17–1.56, i.e. $n' = 1.08$–1.32,

Table 1. Experimental polarizabilities values for common molecular groups from the literature [99].

Group	α (Å^3)	Group	α (Å^3)
–COOH	2.86	–SH	3.47
$-CH_3$	2.24	–CN	2.16
$-CH_2-$	1.84	$-NH_2$	1.76
–C=O	1.82	H_2O	1.45

Table 2. Simulation of local field factors ϵ' and n' with the α value between 2 and 4 Å^3. The case for $\alpha = 1.5$ Å^3 is the simulation results of the interfacial water molecules.

α (Å^3)	a (Å)	$l_{xx} = l_{yy}$	l_{zz}	ϵ'	n'
2.0	4.5	1.11	0.84	1.33	1.15
2.0	5.5	1.06	0.90	1.17	1.08
4.0	4.5	1.25	0.72	1.74	1.32
4.0	5.5	1.12	0.82	1.37	1.17
1.5	3.5	1.19	0.76	1.56	1.25
1.5	4.0	1.12	0.83	1.36	1.16

depending on the lattice constant and the value of the polarizability. The commonly used value $n' = 1.18$ is just around the mid-point.

In the above calculation we assumed that the monolayer is closely packed. If the interfacial monolayer is sparse, the local field effect should be small. However, for the situation of submonolayer adsorption at the liquid–liquid interface, the dipole interactions of the solvent molecules in the interface plane need to be considered. Thus, these n' values are generally in between the vacuum and the substrate dielectric constant, as used in the literature. They are also close to the estimation made by Zhuang *et al.* using a modified Lorentz model of the interface [54], and the simple average of the optical constant of the two adjacent isotropic bulk phases [53,61,71]. However, even though these values worked almost fine, the models and the reasoning behind it prevented the treatment of the different molecular groups at the molecular interface. With the development of laser techniques and the measurement methodology in surface SHG and SFG-VS [1,2,40,41], now such detailed difference can be measured in careful experiments. This should provide new opportunities for the interface studies.

Of course the above simple estimation does not include the bigger chromophores, such as phenyl, biphenyl, etc. Their polarizability is generally much larger, and the local field effects can be much stronger when they are closely aligned at the interface. According to Equation (13), it is possible to have $l_{xx} = l_{yy}$ to be smaller than unity or even go to negative values, and l_{zz} to be larger than unity, when the molecules with relatively large linear polarizability are closely packed even far from resonance. These are unique phenomena for the two-dimensional anisotropic local field factors. According to the Lorentz relation, this is not possible for optical bulk materials with normal dispersion. Such phenomena certainly have yet to be explored experimentally.

The local field factors in the molecular layer are dependent on the orientation and also on how the segmentation is done, and one generally does not have detailed knowledge of this information before knowing the local field factors. Therefore, different approximation approaches were employed in past SHG and SFG-VS studies. Similar to what Munn *et al.* did previously [49,86–89], we invoked the planewise dipole sum rule here to show that in calculating the local field factors using the microscopic point-dipole model with the formulae in Equation (13), extreme care must be taken in order not to overestimate the local field effects. However, this does not imply that the sphere bead model always generates more reasonable results for the local field factors. We want to point out that when the square lattice constant is close to or even smaller than the size of the molecule under studying, the simple point-dipole model is expected to break down, and the planewise dipole sum rule can be used as the remedy. One expects that there is no simple rule to segment the chain molecules in calculating the local field factors. Down to the detailed molecular level, a quantum mechanic treatment of the electron density and their polarizability should be employed to give a more accurate description of the molecules at the interface. Nevertheless, the above estimation can give reasonable upper and lower bounds for the local field factors.

5.3. *SHG or SFG-VS experiments to test the microscopic model*

Here we discuss how SHG and SFG-VS experiments can be used to test the microscopic model.

The key point raised in this study is that the molecular optics treatment of the interface nonlinear radiation can provide a detailed microscopic description of the nonlinear optical processes and the molecular behaviour at the interface. The key to testing the microscopic model is to find a way to determine the microscopic local field factors or to quantitatively determine their effects in the SHG or SFG-VS experiment, and to compare these experimental effects with the molecular details in the molecular monolayer.

There have been few attempts to try to experimentally determine the interfacial effective optical constants with SHG [61,71] and SFG-VS [70]. All of them concluded with a value close to the simple arithmetic average of the optical constant of the two adjacent bulk phases. These works were not based on the microscopic model and they cannot be used to test the microscopic model. This is because the microscopic model predicts that the local field factors, which are connected to the effective optical constant of the interface layer through the relationship $\varepsilon' = n'^2 = l_{yy}/l_{zz}$ [42,54], must depend on the detailed structure of the molecular monolayer and may have values other than the simple arithmetic average or the prediction with the modified macroscopic Lorentz model of the interface [54].

The first test is to determine the local field factor l_{yy}/l_{zz} for the closely packed Langmuir monolayers at the air–water interface with large chromophores. According to Equation (13), when $\alpha_{ii} \sim 15\,\text{Å}^3$ and $a^2 \sim 40\,\text{Å}^2$, one has $\varepsilon' = l_{yy}/l_{zz} \sim 2.10$, thus $n' \sim 1.45$. These kinds of conditions can be easily satisfied with chromophores with two or three phenyl groups, such as alkyl cyano-biphenyl (nCB) or alkyl cyano-triphenyl (nCT) Langmuir films. It has been shown that in the closely packed 8CB Langmuir monolayer at the air–water interface, since the molecular surface density is always known, a self-consistent analysis of the polarization dependent SHG data at different surface densities can give the molecular orientation angle and the ε' value at different surface densities [37,111]. Such self-consistent analysis was suggested by Munn *et al.* before, because they realized that the determination of the molecular orientational angle and the determination of the interface local field factor are interconnected [87]. Such a self-consistent analysis can only be carried out for Langmuir or Langmuir–Blodgett monolayers because their surface densities are known and can be varied controllably. It turned out in our SHG studies that for the 8CB monolayer, ε' changes from 1.7 to 2.4 when the surface density changes from $51\,\text{Å}^2$ to $39\,\text{Å}^2$ per molecule [110,111]. These results agree very well with Equation (13), and the orientational angle thus obtained agrees well with the rod model of the chromophore. This is a very convincing example to show that the local field factors of the molecular monolayer do not have simple values close to the arithmetic average of the two adjacent bulk phases. The details of this study are to be published elsewhere [110,111].

Another test can be designed with the SFG-VS measurement of small rigid linear molecules, such as the acetonitrile molecule, at the air–liquid interface. For example, SFG-VS can selectively measure polarization-dependent vibrational spectra of both the $-CH_3$ and the –CN groups of the interface acetonitrile molecule [113]. Since the molecule is linear, the orientation angles, which are dependent on the values of ε'_{-CN} and ε'_{-CH_3}, respectively, determined from the SFG-VS data of the $-CH_3$ and the –CN groups, should have the same value. Thus the ratio $\varepsilon'_{-CN}/\varepsilon'_{-CH_3}$ can be determined experimentally, without knowing the details of the interface molecular structure. Using the polarization null angle method in SFG-VS [1,114–117], the ratio of the local field factor for the $-CH_3$ and the –CN groups, i.e. $\varepsilon'_{-CN}/\varepsilon'_{-CH_3}$, can be obtained quite accurately from the

experimental data. These two values are indeed significantly different from unity and it is beyond the experimental error bar. This observation cannot be explained by the previous models, but can be well explained and quantitatively analysed with microscopic molecular optics theory as presented in this work, and the structure of the interfacial adsorbed molecular layer. The details of the experimental study and analysis are going to be reported elsewhere [118].

More SHG or SFG-VS experiments can be designed accordingly to test the microscopic model. With the microscopic molecular optics theory of SHG and SFG-VS, detailed analysis of SHG and SFG-VS data is now possible with the recent development of quantitative polarization and configuration dependent measurements in SHG and SFG-VS [1,2,40,41,119,120]. These studies can not only provide a test for the microscopic model, but can also provide detailed information of the molecular interface according to the microscopic model.

6. Concluding remarks

The aim of this work is to present a coherent description of the microscopic theory of surface nonlinear optical spectroscopy for solving practical problems in understanding the details of the molecular interface. SHG and SFG-VS have been proven to be sensitive enough to probe interfacial adsorbates with submonolayer coverage [4,6,11,12]. Therefore, the macroscopic theory treating the submonolayer interface as a separate entity, i.e. the infinitesimally thin polarization layer, is in question. To address this question, the treatment based on the more realistic discrete induced dipole lattice model is thus described in this report. Recent developments in the quantitative polarization and symmetry analysis in SHG and SFG-VS have provided new opportunities in quantitative interface studies [1,2]. These developments also provided more accurate data to test the SHG and the SFG-VS theories at the detailed molecular level [37,40,41,54,61].

The microscopic molecular optics theory of the surface SHG and SFG-VS for the monolayer and submonolayer is based on the treatment of the molecular interface with the realistic discrete induced dipole lattice model. In this theory, the following derivations are presented and discussed: (a) the detailed expressions of the local field factors in the interface molecular layer; (b) the detailed expressions for the far-field radiation of the SHG as well as the SFG-VS process from the interface induced dipoles. It turned out that the asymptotic results for the far-field radiation has the same form as the results derived from the macroscopic infinitesimally thin polarization sheet layer treatment first developed by Heinz and Shen in the early 1980s using the Maxwell equations with boundary conditions [6,57], as well as later modifications with the consideration of the microscopic local field factors using the classical dipole model [42,54,59].

Microscopic molecular optics theory of surface SHG and SFG-VS is capable of providing more detailed microscopic–molecular level information of the molecular interface. According to Born and Wolf, molecular optics theory directly connects macroscopic optical phenomena to molecular properties, and can provide deeper physical insight into electromagnetic interaction problems than does the rather formal approach based on Maxwell's phenomenological equations [55,56]. Based on the microscopic and

discrete induced dipole lattice model, the problem of the macroscopic dielectric constants of the interfacial molecular monolayer is discussed and clarified. The macroscopic dielectric constant of the molecular submonolayer and monolayer needed in the macroscopic theory is no longer an issue in the microscopic model of the surface nonlinear optics.

In their classic paper on nonlinear optics, Bloembergen and Pershan [35] showed that the approach using the integral equation based on the Ewald–Oseen extinction theorem reached exactly the same results for the nonlinear response from the nonlinear plate parallel slab [35,91]. Since in that work the slab was treated as a continuous medium, the molecular optics approach was more complex and was simply redundant to the macroscopic theory, i.e. no additional physical insight was reached beyond the macroscopic approach. In contrast, when the microscopic molecular optics approach is combined with the discrete dipole lattice model, it can directly connect the microscopic molecular properties and the macroscopic optical phenomenon. The benefit is not only the consistency in the theoretical treatment as discussed above, but also the possibility of having a microscopic molecular theory for the surface nonlinear optics for future applications in understanding the molecular level details at the molecular interface.

Based on the planewise dipole sum rule and the previous work by Munn *et al.*, the issue of how the microscopic local field factors can be evaluated was also discussed. According to these results, the effectiveness and limit of the simple point-dipole lattice model on the quantitative evaluation of the effective dielectric constant of the interfacial molecular monolayer are discussed and evaluated. For simple and small molecular groups, the simple point-dipole lattice model does provide a good approximation of the microscopic local field effects of the interfacial molecular monolayer. The SHG and SFG-VS experimental tests of the microscopic discrete dipole lattice model are also discussed. With these developments, many previous SHG and SFG-VS studies can be better understood and evaluated. Moreover, these developments can provide a full microscopic description of the nonlinear radiation from the molecular interface. Detailed molecular information can be obtained from the model developed in this work, together with better and more accurate polarization measurement data in SHG and SFG-VS.

Furthermore, it is to be remembered that the microscopic model of the interface is not limited to the two-dimensional point-dipole lattice model. The microscopic molecular optics theory allows the incorporation of different microscopic interface models. This allows detailed studies of the interface structure at the microscopic level, without being annoyed by the issue of the undefinable macroscopic dielectric constant of the interface layer.

The microscopic molecular optics approach can also be applied to the treatment of the ellipsometry response and polarized ATR-FTIR spectroscopy from molecular monolayer interfaces and thin films. When ellipsometry and polarized ATR-FTIR are to be applied to study such interfaces and films, a microscopic molecular theory for the ellipsometry and polarized ATR-FTIR is certainly needed. So far, the treatment of the ellipsometry or polarized ATR-FTIR and the treatment of the SHG or SFG-VS are not fully consistent in their description of the anisotropy in the molecular layer. We shall discuss these issues elsewhere.

In conclusion, an effective microscopic molecular optics theory as described in this report may shed new light on both linear and nonlinear optics interface studies.

Acknowledgements

DSZ acknowledges the helpful discussion from Wen-kai Zhang, Yu-jie Sun and Yuan Guo. HFW thanks Yan-yan Xu for deriving the expression in Equation (45) and her help on a revision of this manuscript. HFW also acknowledges support by the Natural Science Foundation of China (NSFC, No. 20425309, No. 20533070, No. 20773143) and the Ministry of Science and technology of China (MOST No. 2007CB815205).

References

[1] H. F. Wang, W. Gan, R. Lu, Y. Rao, and B. H. Wu, Int. Rev. Phys. Chem. **24**, 191 (2005).
[2] W. K. Zhang, H. F. Wang, and D. S. Zheng, Phys. Chem. Chem. Phys. **8**, 4041 (2006).
[3] Y. R. Shen, Ann. Rev. Mat. Sci. **16**, 69 (1986).
[4] Y. R. Shen, Nature **337**, 519 (1989).
[5] G. L. Richmond, J. M. Robinson, and V. L. Shannon, Prog. Surf. Sci. **28**, 1 (1988).
[6] Y. R. Shen, Annu. Rev. Phys. Chem. **40**, 327 (1989).
[7] V. Vogel and Y. R. Shen, Annu. Rev. Mat. Sci. **21**, 515 (1991).
[8] K. B. Eisenthal, Acc. Chem. Res. **26**, 636 (1993).
[9] C. D. Bain, J. Chem. Soc. Faraday Trans. **91**, 1281 (1995).
[10] K. B. Eisenthal, Annu. Rev. Phys. Chem. **43**, 627 (1992).
[11] R. M. Corn and D. A. Higgins, Chem. Rev. **94**, 107 (1994).
[12] K. B. Eisenthal, Chem. Rev. **96**, 1343 (1996).
[13] P. B. Miranda and Y. R. Shen, J. Phys. Chem. B **103**, 3292 (1999).
[14] G. A. Somorjai and G. Rupprechter, J. Phys. Chem. B **103**, 1623 (1999).
[15] M. J. Shultz, C. Schnitzer, D. Simonelli, and S. Baldelli, Int. Rev. Phys. Chem. **19**, 123 (2000).
[16] Y. R. Shen, IEEE J. Sel. Top. Quant. Elec. **6**, 1375 (2000).
[17] G. L. Richmond, Annu. Rev. Phys. Chem. **52**, 357 (2001).
[18] M. Buck and M. Himmelhaus, J. Vac. Sci. Tech. A **19**, 2717 (2001).
[19] Y. R. Shen, Pure Appl. Chem. **73**, 1589 (2001).
[20] G. L. Richmond, Chem. Rev. **102**, 2693 (2002).
[21] Z. Chen, Y. R. Shen, and G. A. Somorjai, Annu. Rev. Phys. Chem. **53**, 437 (2002).
[22] F. Vidal and A. Tadjeddine, Rep. Prog. Phys. **68**, 1095 (2005).
[23] Y. R. Shen and V. Ostroverkhov, Chem. Rev. **106**, 1140 (2006).
[24] S. Gopalakrishnan, D. F. Liu, H. C. Allen, M. Kuo, and M. J. Shultz, Chem. Rev. **106**, 1155 (2006).
[25] K. B. Eisenthal, Chem. Rev. **106**, 1462 (2006).
[26] Y. R. Shen, *The Principles of Nonlinear Optics* (John Wiley, New York, 2003), Chapter 25.
[27] C. K. Chen, A. R. B. Decastro, and Y. R. Shen, Phys. Rev. Lett. **46**, 145 (1981).
[28] T. F. Heinz, C. K. Chen, D. Ricard, and Y. R. Shen, Phys. Rev. Lett. **48**, 478 (1982).
[29] T. F. Heinz, H. W. K. Tom, and Y. R. Shen, Phys. Rev. A **28**, 1883 (1983).
[30] Y. R. Shen, J. Vac. Sci. Tech. B **3**, 1464 (1985).
[31] P. Guyot-sionnest, W. Chen, and Y. R. Shen, Phys. Rev. B **33**, 8254 (1986).
[32] X. D. Zhu, H. Suhr, and Y. R. Shen, Phys. Rev. B **35**, 3047 (1987).
[33] P. Guyot-Sionnest, R. Superfine, J. H. Hunt, and Y. R. Shen, Chem. Phys. Lett. **144**, 1 (1988).
[34] M. B. Feller, W. Chen, and Y. R. Shen, Phys. Rev. A **43**, 6778 (1991).
[35] N. Bloembergen and P. S. Pershan, Phys. Rev. **128**, 606 (1962).
[36] G. J. Simpson and K. L. Rowlen, Acc. Chem. Res. **33**, 781 (2000).
[37] Y. Rao, Y. S. Tao, and H. F. Wang, J. Chem. Phys. **119**, 5226 (2003).
[38] M. J. Shultz, *Advances in Multiphoton Process and Spectroscopy*, edited by S. H. Lin, A. A. Villaeys, and Y. Fujimura (World Scientific, Singapore, 2008), Vol. 18.
[39] W. Gan, D. Wu, Z. Zhang, R. R. Feng, and H. F. Wang, J. Chem. Phys. **124**, 114705 (2006).

[40] W. Gan, B. H. Wu, Z. Zhang, Y. Guo, and H. F. Wang, J. Phys. Chem. C **111**, 8716 (2007).
[41] W. Gan, Z. Zhang, R. R. Feng, and H. F. Wang, J. Phys. Chem. C **111**, 8726 (2007).
[42] X. Wei, S. C. Hong, X. W. Zhuang, T. Goto, and Y. R. Shen, Phys. Rev. E **62**, 5160 (2000).
[43] L. M. Hayden, Phys. Rev. B **38**, 3718 (1988).
[44] J. F. McGilp, Z. R. Tang, and M. Cavanagh, Syn. Met. **61**, 181 (1993).
[45] G. Cnossen, K. E. Drabe, D. A. Wiersma, M. A. Schoondorp, A. J. Schouten, J. B. E. Hulshof, and B. L. Feringa, Langmuir **9**, 1974 (1993).
[46] Z. R. Tang, M. Cavanagh, and J. F. McGilp, J. Phys.: Cond. Matt. **5**, 3791 (1993).
[47] G. Cnossen, K. E. Drabe, and D. A. Wiersma, J. Chem. Phys. **97**, 4512 (1992).
[48] H. Ui, A. Tomioka, T. Nishiwaki, and K. Miyano, J. Chem. Phys. **101**, 6430 (1994).
[49] R. W. Munn and M. M. Shabat, J. Chem. Phys. **99**, 10059 (1993).
[50] E. Mishina, Y. Miyakita, Q. K. Yu, S. Nakabayashi, and H. Sakaguchi, J. Chem. Phys. **117**, 4016 (2002).
[51] T. G. Zhang, C. H. Zhang, and G. K. Wong, J. Opt. Soc. Am. B **7**, 902 (1990).
[52] F. Eisert, O. Dannenberger, and M. Buck, Phys. Rev. B **58**, 10860 (1998).
[53] J. A. Ekhoff and K. L. Rowlen, Anal. Chem. **74**, 5954 (2002).
[54] X. Zhuang, P. B. Miranda, D. Kim, and Y. R. Shen, Phys. Rev. B **59**, 12632 (1999).
[55] E. Lalor and E. Wolf, J. Opt. Soc. Am. **62**, 1165 (1972).
[56] M. Born and E. Wolf, *Principles of Optics: Electromagnetic Theory of Propagation, Interference and Diffraction of Light*, 6th ed. (Cambrige Unverisity Press, Cambrige, 1997), pp. 38–41, 81–84; 104–108.
[57] T. F. Heinz, PhD dissertation, *Nonlinear Optics of Surfaces and Interfaces,* Univeristy of California, Berkeley, 1982.
[58] T. F. Heinz, in *Nonlinear Surface Electromagnetic Phenomena*, edited by H. E. Ponath and G. I. Stegman (North-Holland, Armsterdam, 1991), pp. 353–416.
[59] P. X. Ye and Y. R. Shen, Phys. Rev. B **28**, 4288 (1983).
[60] D. Roy, Phys. Rev. B **61**, 13283 (2000).
[61] G. J. Simpson, C. A. Dailey, R. M. Plocinik, A. J. Moad, M. A. Polizzi, and R. M. Everly, Anal. Chem. **77**, 215 (2005).
[62] R. M. A. Azzam and N. M. Bashara, *Ellipsometry and Polarized Light* (Elsevier, Amsterdam, 1987).
[63] O. S. Heavens, *Optical Properties of Thin Solid Films* (Dover, New York, 1991).
[64] P. Guyot-sionnest, Y. R. Shen, and T. F. Heinz, Appl. Phys. B **42**, 237 (1987).
[65] N. Bloembergen, *Nonlinear Optics* (Benjamin, New York, 1965), p. 69.
[66] D. Lupo, W. Prass, U. Scheunemann, A. Laschewsky, H. Ringsdorf, and I. Ledoux, J. Opt. Soc. Am. B **5**, 300 (1988).
[67] H. Hsiung, G. R. Meredith, H. Vanherzeele, R. Popovitzbiro, E. Shavit, and M. Lahav, Chem. Phys. Lett. **164**, 539 (1989).
[68] J. E. Sipe, J. Opt. Soc. Am. B **4**, 481 (1987).
[69] V. Mizrahi and J. E. Sipe, J. Opt. Soc. Am. B **15**, 660 (1988).
[70] J. Wang, Z. Paszti, M. A. Even, and Z. Chen, J. Phys. Chem. B **108**, 3625 (2004).
[71] J. G. Frey, Chem. Phys. Lett. **323**, 454 (2000).
[72] R. R. Naujok, H. J. Paul, and R. M. Corn, J. Phys. Chem. **100**, 10497 (1996).
[73] D. A. Higgins, M. B. Abrams, S. K. Byerly, and R. M. Corn, Langmuir **8**, 1994 (1992).
[74] R. Braun, B. D. Casson, and C. D. Bain, Chem. Phys. Lett. **245**, 326 (1995).
[75] M. J. Citra and P. H. Axelsen, Biophy. J. **71**, 1796 (1996).
[76] P. H. Axelsen and M. J. Citra, Prog. Biophys. Mol. Biol. **66**, 227 (1996).
[77] L. K. Tamm and S. A. Tatulian, Quart. Rev. Biophy. **30**, 365 (1997).
[78] E. Goormaghtigh, V. Raussens, and J.-M. Ruysschaert, Biochim. Biophys. Acta **1422**, 105 (1999).
[79] R. W. Munn, J. Chem. Phys. **103**, 850 (1995).

[80] F. W. Wette and G. E. Schacher, Phys. Rev. **137**, A78 (1965).
[81] C. D. Mahan and G. Obermair, Phys. Rev. **183**, 834 (1969).
[82] M. R. Philpott, J. Chem. Phys. **56**, 996 (1972).
[83] M. R. Philpott, J. Chem. Phys. **58**, 588 (1973).
[84] M. R. Philpott and J. W. Lee, J. Chem. Phys. **58**, 595 (1973).
[85] M. R. Philpott, J. Chem. Phys. **61**, 5306 (1974).
[86] M. I. H. Panhuis and R. W. Munn, J. Chem. Phys. **112**, 6763 (2000).
[87] M. I. H. Panhuis and R. W. Munn, J. Chem. Phys. **112**, 10691 (2000).
[88] M. I. H. Panhuis and R. W. Munn, J. Chem. Phys. **112**, 10685 (2000).
[89] R. W. Munn and M. M. Shabat, J. Chem. Phys. **99**, 10052 (1993).
[90] A. V. Ghiner and G. I. Surdutovich, Phys. Rev. A **49**, 1313 (1994).
[91] J. A. Armstrong, N. Bloembergen, J. Ducuing, and P. S. Pershan, Phys. Rev. **127**, 1918 (1962).
[92] N. Bloembergen, IEEE J. Sel. Top. Quant. Electron. **6**, 876 (2000).
[93] A. Bagchi, R. G. Barrera, and B. B. Dasgupta, Phys. Rev. Lett. **44**, 1475 (1980).
[94] A. Bagchi, R. G. Barrera, and R. Fuchs, Phys. Rev. B **25**, 7086 (1982).
[95] M. Iwamoto, Y. Mizutani, and A. Sugimura, Phys. Rev. B **54**, 8186 (1996).
[96] J. Topping, Proc. R. Soc. London, A **114**, 67 (1927).
[97] C. Hirose, N. Akamatsu, and K. Domen, Appl. Spec. **46**, 1051 (1992).
[98] K. J. Miller and J. A. Savchik, J. Am. Chem. Soc. **101**, 7206 (1979).
[99] K. J. Miller, J. Am. Chem. Soc. **112**, 8533 (1990).
[100] K. J. Miller, J. Am. Chem. Soc. **112**, 8543 (1990).
[101] R. W. Boyd, *Nonlinear Optics* (Academic Press, New York, 1992), p. 65.
[102] P. F. Brevet, *Surface Second Harmonic Generation* (Press Polytechniques et Universitaires Romandes, Lausanne, 1997).
[103] W. K. Zhang, D. S. Zheng, Y. Y. Xu, H. T. Bian, Y. Guo, and H. F. Wang, J. Chem. Phys. **123**, 224713 (2005).
[104] J. J. Maki, M. Kauranen, and A. Persoons, Phys. Rev. B **51**, 1425 (1995).
[105] R. M. Townsend and S. A. Rice, J. Chem. Phys. **94**, 2207 (1991).
[106] A. Braslau, M. Deutsch, P. S. Pershan, A. H. Weiss, J. Als-Nielsen, and J. Bohr, Phys. Rev. Lett. **54**, 114 (1985).
[107] A. Braslau, P. S. Pershan, G. Swislow, B. M. Ocko, and J. Als-Nielsen, Phys. Rev. A **38**, 2457 (1988).
[108] A. Biadasz, T. Martyniski, R. Stolarski, and D. Bauman, Liq. Crys. **31**, 1639 (2004).
[109] R. Hertmanowski, T. Martyniski, and D. Bauman, J. Mol. Struc. **741**, 201 (2005).
[110] D. S. Zheng, PhD dissertation, *Investigation of Orientational Phase Transition of Liquid-Crystal Langmuir Monolayers at Air/Water Interface by Second Harmonic Generation and Treatment on Two-Dimensional Local Field Effect* Institute of Chemistry, Chinese Academy of Sciences, Beijing, 2006.
[111] D. S. Zheng and H. F. Wang, unpublished work.
[112] J. Wang, C. Chen, S. M. Buck, and Z. Chen, J. Phys. Chem. B **105**, 12118 (2001).
[113] D. Zhang, J. H. Gutow, and K. B. Eisenthal, J. Chem. Phys. **98**, 5099 (1993).
[114] W. Gan, B. H. Wu, H. Chen, Y. Guo, and H. F. Wang, Chem. Phys. Lett. **406**, 467 (2005).
[115] R. Lu, W. Gan, and H. F. Wang, Chin. Sci. Bull. **48**, 2183 (2003).
[116] R. Lu, W. Gan, and H. F. Wang, Chin. Sci. Bull. **49**, 899 (2004).
[117] H. Chen, W. Gan, B. H. Wu, D. Wu, Z. Zhang, and H. F. Wang, Chem. Phys. Lett. **408**, 284 (2005).
[118] Z. Zhang and H. F. Wang, unpublished work.
[119] R. M. Plocinik, R. M. Everly, A. J. Moad, and G. J. Simpson, Phys. Rev. B **72**, 125409 (2005).
[120] R. M. Plocinik and G. J. Simpson, Anal. Chim. Acta **496**, 133 (2003).